

# Matrix-Calibration-Based Cascaded Channel Estimation for Reconfigurable Intelligent Surface Assisted Multiuser MIMO

Hang Liu, Xiaojun Yuan, *Senior Member, IEEE*, and Ying Jun  
(Angela) Zhang, *Senior Member, IEEE*

## Abstract

Reconfigurable intelligent surface (RIS) is envisioned to be an essential component of the paradigm for beyond 5G networks as it can potentially provide similar or higher array gains with much lower hardware cost and energy consumption compared with the massive multiple-input multiple-output (MIMO) technology. In this paper, we focus on one of the fundamental challenges, namely the channel acquisition, in an RIS-assisted multiuser MIMO system. The state-of-the-art channel acquisition approach in such a system with fully passive RIS elements estimates the cascaded transmitter-to-RIS and RIS-to-receiver channels by adopting excessively long training sequences. To estimate the cascaded channels with an affordable training overhead, we formulate the channel estimation problem in the RIS-assisted multiuser MIMO system as a matrix-calibration based matrix factorization task. By exploiting the information on the slow-varying channel components and the hidden channel sparsity, we propose a novel message-passing based algorithm to factorize the cascaded channels. Furthermore, we present an analytical framework to characterize the theoretical performance bound of the proposed estimator in the large-system limit. Finally, we conduct simulations to verify the high accuracy and efficiency of the proposed algorithm.

## Index Terms

Channel estimation, reconfigurable intelligent surface, multiuser MIMO, matrix factorization, matrix calibration, message passing, replica method.

H. Liu and Y. J. Zhang are with the Department of Information Engineering, The Chinese University of Hong Kong, Shatin, New Territories, Hong Kong SAR (e-mail: lh117@ie.cuhk.edu.hk; yjzhang@ie.cuhk.edu.hk). X. Yuan is with the Center for Intelligent Networking and Communications, the University of Electronic Science and Technology of China, Chengdu, China (e-mail: xjyuan@uestc.edu.cn).

## I. INTRODUCTION

As one of the key techniques of the fifth-generation (5G) wireless networks, massive multiple-input multiple-output (MIMO) can greatly enhance system throughput and enlarge cell coverage. However, expensive hardware cost and high power consumption are two unresolved challenges in current massive MIMO systems [1]. Substitute technologies have been explored to achieve more sustainable and more reliable communications for the next generation mobile networks. Among these new technologies, reconfigurable intelligent surface (RIS) assisted MIMO [2]–[4] is deemed very promising to realize similar or even higher array gains with significant cost reduction compared with massive MIMO. Comprising a large number of reconfigurable reflecting elements that can induce adjustable and independent phase shifts on the incident signals, an RIS is able to constructively combine the reflected signals to achieve a high level of energy focusing at the receiver side. Due to the passive and low-cost nature of the reflecting elements, the RIS requires very low energy consumption and is easy to be integrated into the existing wireless systems [5].

In recent years, the design of RISs to assist wireless communications has attracted extensive attention. To name a few, the authors in [5]–[7] employ RISs to control the propagation environment and improve the coverage for indoor communications. In [2]–[4], [8], [9], the authors propose various methods to configure the RIS phase shifts in outdoor communications, in order to optimize different communication utilities. It is worth noting that accurate channel state information (CSI) is critical in optimizing the RIS parameters. Unfortunately, all the aforementioned work assumes perfect CSI without considering its acquisition difficulty. In fact, channel estimation in an RIS-assisted wireless system is much more challenging than in a conventional system. This is because the passive RIS elements are incapable of sensing and estimating channel information. Therefore, we shall rely on the receiver to estimate both the transmitter-to-RIS and RIS-to-receiver channels by observing only a noisy cascade of the two channels.

To address the channel estimation challenge in RIS-assisted communication systems, some pioneering work has recently emerged. For example, Ref. [10] assumes that the RIS elements are fully active and are connected to a signal processing unit to perform channel estimation. Similarly, Ref. [11] requires a portion of the RIS elements to be active so that the channels of the passive elements can be inferred via a compressed-sensing based approach. Compared with active RIS

elements, purely passive RIS elements are undoubtedly more appealing due to their extremely low hardware and deployment costs. Ref. [12], [13] show that channel estimation in passive-RIS-assisted systems can be converted into a sequence of conventional MIMO channel estimation problems by turning on one RIS element at a time. However, the training overhead of this method is proportional to the size of the RIS and may be prohibitively large as the RIS typically comprises a large number of elements. As such, the following question arises naturally: *How to estimate the two cascaded channels with purely passive reflecting elements and an affordable training overhead?* A preliminary answer to this question appears in the recent work [14], where the authors develop a cascaded channel estimation algorithm for an RIS-assisted *single-user* MIMO system. Specifically, Ref. [14] formulates the cascaded channel estimation problem as a combination of sparse matrix factorization and low-rank matrix completion by leveraging the programmable property of the RIS and the low-rankness of the propagation channel.

In this paper, we consider the cascaded channel estimation problem for an RIS-assisted *multiuser* MIMO system, where a fully passive RIS is used to assist the communication. In practice, the RIS can be coated onto a wall, a ceiling, or a furniture in an indoor environment; or mounted on a building facade, an advertising panel, a traffic sign, or a highway fence in an outdoor environment. In a typical application scenario, both the BS and the RIS rarely move after deployment. As a result, the channel between the BS and the RIS can be modelled as a quasi-static end-to-end MIMO channel, in which most of the channel components evolve much more slowly compared with conventional mobile communication channels. Meanwhile, a small portion of the channel components of the BS-to-RIS channel may experience sudden changes. For example, an opening/closing of a door in an indoor scenario or a moving car in an outdoor scenario may change the scattering geometry. Likewise, an offset of the antennas at either end may change the array response. By modeling both the fast and slow varying channel components, we formulate the CSI acquisition problem as a *matrix-calibration-based matrix factorization* task. Then, we propose a novel message-passing based algorithm to effectively estimate the two cascaded channels. Besides, we present an analytical framework to analyze the performance of the considered system. The main contributions of this paper are summarized as follows.

- We characterize the slow-varying and fast-varying channel components of the BS-to-RIS channel link by the Rician fading model. Unlike [14] that assumes the low-rankness of the BS-to-RIS channel matrix, we exploit the information on the slow-varying channel

components for channel estimation. Specifically, we assume that the slow-varying channel components can be estimated by long-term channel averaging prior to the RIS channel estimation procedure. Based on this assumption, we formulate the cascaded channel estimation problem as a joint task of the BS-to-RIS channel matrix calibration and the RIS-to-user channel matrix estimation.

- We develop the posterior mean estimators under the Bayesian inference framework to infer the two cascaded channels and adopt the sum-product message passing algorithm to approximately compute the estimators. We show that direct computation of the messages may lead to prohibitively high complexity. To tackle this challenge, we introduce additional approximations to the messages based on the approximate message passing (AMP) framework [15], [16]. The proposed algorithm only needs to update the means and variances of the messages and hence avoids high-dimensional integrations in the canonical message passing algorithm. Furthermore, we exploit the inherent channel sparsity in the angular domain by over-complete sampling bases to enhance the estimation accuracy.
- Based on the replica method from statistical physics [17], we analyze the asymptotic performance of the posterior mean estimators in the large-system limit. We show that with perfect knowledge of the channel prior distributions under some appropriately chosen angle sampling bases, the mean square errors (MSEs) of the posterior mean estimators can be determined by the fixed point of a set of scalar equations. We further show by numerical simulations that the proposed approximate channel estimators can closely approach the replica method bound.

The remainder of this paper is organized as follows. In Section II, we describe the RIS-assisted multiuser MIMO system model and the cascaded channel estimation problem. In Section III, we develop the channel estimation algorithm and introduce additional approximations to reduce the computational complexity. In Section IV, we perform asymptotic analysis based on the replica method. Section V presents extensive numerical results of the proposed method, and the paper concludes in Section VI.

*Notation:* Throughout, we use  $\mathbb{C}$  and  $\mathbb{R}$  to denote the real and complex number sets, respectively. Regular letters, bold small letters, and bold capital letters are used to denote scalars, vectors, and matrices, respectively. We use  $j \triangleq \sqrt{-1}$  to denote the imaginary unit. We use  $(\cdot)^*$ ,  $(\cdot)^T$ , and  $(\cdot)^H$  to denote the conjugate, the transpose, and the conjugate transpose, respectively. We use  $x_{ij}$  to denote the  $(i, j)$ -th entry of  $\mathbf{X}$ . We use  $\mathcal{N}(\cdot; \boldsymbol{\mu}, \boldsymbol{\Sigma})$  and  $\mathcal{CN}(\cdot; \boldsymbol{\mu}, \boldsymbol{\Sigma})$  to denote

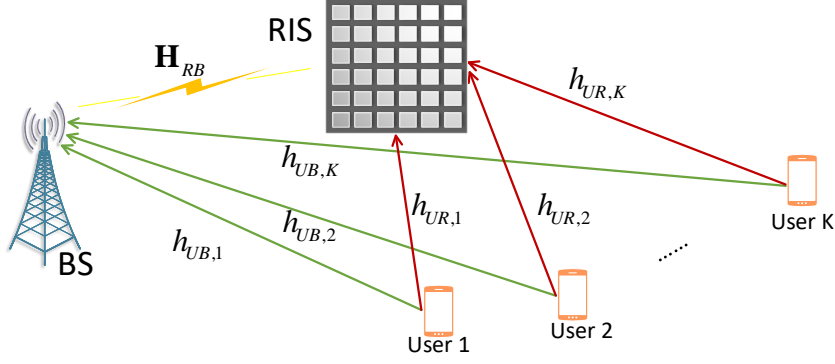


Fig. 1. An RIS-assisted multiuser system.

the real normal and the circularly-symmetric normal distributions with mean  $\boldsymbol{\mu}$  and covariance  $\boldsymbol{\Sigma}$ , respectively. We use  $\text{tr}(\mathbf{X})$  to denote the trace of  $\mathbf{X}$ ,  $\text{rank}(\mathbf{X})$  to denote the rank of  $\mathbf{X}$ ,  $\mathbf{I}$  to denote the identity matrix with an appropriate size,  $\text{diag}(\mathbf{x})$  to denote a diagonal matrix with the diagonal entries specified by  $\mathbf{x}$ , and  $\mathbf{1}$  to denote the all-one vector with an appropriate size. We use  $\|\cdot\|_p$  to denote the  $\ell_p$  norm,  $\|\cdot\|_F$  to denote the Frobenius norm,  $\delta(\cdot)$  to denote the Dirac delta function,  $\propto$  to denote equality up to a constant multiplicative factor, and  $\mathbb{E}[\cdot]$  to denote the expectation operator.

## II. SYSTEM MODEL AND PROBLEM FORMULATION

### A. RIS-Assisted Multiuser MIMO

Consider a single-cell RIS-assisted multiuser MIMO system depicted in Fig. 1. Assume that  $K$  single-antenna users simultaneously communicate with an  $M$ -antenna BS. An RIS comprising  $L$  phase-shift elements is deployed to assist the communication between the users and the BS. A uniform linear array (ULA) is adopted at the BS, and the passive reflecting elements in the RIS are arranged in the form of an  $L_1 \times L_2$  uniform rectangular array (URA) with  $L_1 L_2 = L$ . Denote by  $\mathbf{h}_{UB,k} \in \mathbb{C}^{M \times 1}$ ,  $\mathbf{h}_{UR,k} \in \mathbb{C}^{L \times 1}$ , and  $\mathbf{H}_{RB} \in \mathbb{C}^{M \times L}$  the channel coefficient vectors/matrix of the  $k$ -th-user-to-BS link, the  $k$ -th-user-to-RIS link, and the RIS-to-BS link, respectively. We assume that the RIS elements induce independent phase shifts on the incident signals. Denote the RIS phase-shift vector at time  $t$  by  $\boldsymbol{\psi}(t) \triangleq [\varpi_1(t)e^{j\psi_1(t)}, \varpi_2(t)e^{j\psi_2(t)}, \dots, \varpi_L(t)e^{j\psi_L(t)}]^T$ , where  $\varpi_l(t) \in \{0, 1\}$  represents the on/off state of the  $l$ -th RIS element, and  $\psi_l(t) \in [0, 2\pi)$  represents the phase shift of the  $l$ -th RIS element.

### B. Channel Model

We assume a quasi-static flat fading channel model, where the channel coefficients remain invariant within the coherence time  $C$ . As discussed in the Introduction, we need to capture both the slow-varying and fast-varying channel components in the RIS-to-BS channel matrix  $\mathbf{H}_{RB}$ . To this end, we model  $\mathbf{H}_{RB}$  by the MIMO Rician fading model as [18]

$$\mathbf{H}_{RB} = \sqrt{\frac{\kappa}{\kappa+1}} \bar{\mathbf{H}}_{RB} + \sqrt{\frac{1}{\kappa+1}} \tilde{\mathbf{H}}_{RB}, \quad (1)$$

where  $\bar{\mathbf{H}}_{RB}$  represents the slow-varying channel components;  $\tilde{\mathbf{H}}_{RB}$  represents the fast-varying channel components due to the change of the propagation geometry or the antenna structure; and  $\kappa$  is the Rician factor denoting the power ratio between the two components.

Moreover, the slow-varying component matrix  $\bar{\mathbf{H}}_{RB}$  sums up the paths from all the deterministic scattering clusters (possibly including the line-of-sight path) and can be modeled as

$$\bar{\mathbf{H}}_{RB} = \sqrt{\beta_0} \sum_{p=1}^{\bar{P}_{RB}} \alpha_p \mathbf{a}_B(\theta_p) \mathbf{a}_R^H(\phi_p, \sigma_p), \quad (2)$$

where  $\beta_0$  is the large-scale path gain encompassing distance-dependent path loss and shadowing;  $\bar{P}_{RB}$  is the number of the slow-varying paths;  $\alpha_p$  is the corresponding complex-valued channel coefficient of the  $p$ -th path;  $\theta_p$  is the corresponding azimuth angle-of-arrival (AoA) at the BS;  $\phi_p$  (or  $\sigma_p$ ) is the corresponding azimuth (or elevation) angle-of-departure (AoD) at the RIS; and  $\mathbf{a}_B$  (or  $\mathbf{a}_R$ ) is the steering vector associated with the BS (or RIS) antenna geometry. In specific,

$$\mathbf{a}_B(\theta) = \frac{1}{\sqrt{M}} \left[ 1, e^{-j\frac{2\pi}{\varrho}d\sin(\theta)}, \dots, e^{-j\frac{2\pi}{\varrho}d(M-1)\sin(\theta)} \right]^T, \quad (3)$$

$$\mathbf{a}_R(\phi, \sigma) = \mathbf{a}_{R,v}(\phi, \sigma) \otimes \mathbf{a}_{R,h}(\phi, \sigma), \quad (4)$$

where  $\varrho$  denotes the carrier wavelength;  $d$  denotes the distance between any two adjacent antennas;  $\otimes$  denotes the Kronecker product; and the horizontal and vertical steering vectors  $\mathbf{a}_{R,h}(\phi, \sigma) \in \mathbb{C}^{L_1 \times 1}$  and  $\mathbf{a}_{R,v}(\phi, \sigma) \in \mathbb{C}^{L_2 \times 1}$  are given by

$$\mathbf{a}_{R,h}(\phi, \sigma) = \frac{1}{\sqrt{L_1}} \left[ 1, e^{-j\frac{2\pi d}{\varrho} \cos(\sigma) \sin(\phi)}, \dots, e^{-j\frac{2\pi d}{\varrho} (L_1-1) \cos(\sigma) \sin(\phi)} \right]^T, \quad (5a)$$

$$\mathbf{a}_{R,v}(\phi, \sigma) = \frac{1}{\sqrt{L_2}} \left[ 1, e^{j\frac{2\pi d}{\varrho} \cos(\sigma) \cos(\phi)}, \dots, e^{j\frac{2\pi d}{\varrho} (L_2-1) \cos(\sigma) \cos(\phi)} \right]^T. \quad (5b)$$

Meanwhile, we represent  $\tilde{\mathbf{H}}_{RB}$  and  $\mathbf{h}_{UR,k}$  as

$$\tilde{\mathbf{H}}_{RB} = \sqrt{\beta_0} \sum_{p=1}^{\tilde{P}_{RB}} \alpha_p \mathbf{a}_B(\theta_p) \mathbf{a}_R^H(\phi_p, \sigma_p), \quad (6)$$

$$\mathbf{h}_{UR,k} = \sqrt{\beta_k} \sum_{p=1}^{P_k} \alpha_p \mathbf{a}_R(\phi_p, \sigma_p), \quad (7)$$

where  $\tilde{P}_{RB}$  is the number of the fast-varying paths;  $\beta_k$  is the large-scale path gain for the channel between the  $k$ -th user and the RIS; and  $P_k$  is the number of paths between the  $k$ -th user and the RIS.

As discussed in the Introduction, we assume that the slow-varying component matrix  $\bar{\mathbf{H}}_{RB}$  in (2) keeps static over a time interval much larger than the coherence block length  $C$ . As a consequence,  $\bar{\mathbf{H}}_{RB}$  can be accurately estimated by long-term channel averaging prior to the RIS channel estimation procedure.<sup>1</sup> Without loss of generality, we assume that  $\text{tr}(\bar{\mathbf{H}}_{RB} \bar{\mathbf{H}}_{RB}^H) = \text{tr}(\tilde{\mathbf{H}}_{RB} \tilde{\mathbf{H}}_{RB}^H) = \beta_0 ML$  and  $\|\mathbf{h}_{UR,k}\|_2^2 = \beta_k L, \forall k$ . In other words,  $\beta_0$  (or  $\beta_k$ ) can be regarded as the average power attenuation for each RIS-BS (or user-RIS) antenna pair.

Following [19], we employ a pre-discretized sampling grid  $\boldsymbol{\vartheta}$  with length  $M'$  ( $\geq M$ ) to discretize  $\{\sin(\theta_p) : 1 \leq p \leq \tilde{P}_{RB}\}$  over  $[0, 1]$ . Similarly, we employ two sampling grids  $\boldsymbol{\varphi}$  with length  $L'_1$  ( $\geq L_1$ ) and  $\boldsymbol{\varsigma}$  with length  $L'_2$  ( $\geq L_2$ ) to discretize  $\{\cos(\sigma_p) \sin(\phi_p) : 1 \leq p \leq \tilde{P}_{RB}\}$  and  $\{-\cos(\sigma_p) \cos(\phi_p) : 1 \leq p \leq \tilde{P}_{RB}\}$ , respectively. Then, we represent the fast-varying component matrix  $\tilde{\mathbf{H}}_{RB}$  under the angular bases as [19]

$$\sqrt{\frac{1}{\kappa + 1}} \tilde{\mathbf{H}}_{RB} = \mathbf{A}_B(\boldsymbol{\vartheta}) \mathbf{S} \left( \underbrace{\mathbf{A}_{R,v}(\boldsymbol{\varsigma}) \otimes \mathbf{A}_{R,h}(\boldsymbol{\varphi})}_{=\mathbf{A}_R(\boldsymbol{\varphi}, \boldsymbol{\varsigma})} \right)^H, \quad (8)$$

where  $\mathbf{A}_B(\boldsymbol{\vartheta}) \triangleq [\mathbf{f}_M(\vartheta_1), \dots, \mathbf{f}_M(\vartheta_{M'})]$  is an over-complete array response with the transform vector  $\mathbf{f}_M(x) \triangleq [1, \dots, e^{-j\frac{2\pi}{\theta} d(M-1)x}]^T / \sqrt{M}$ ;  $\mathbf{A}_{R,h}(\boldsymbol{\varphi}) \triangleq [\mathbf{f}_{L_1}(\varphi_1), \dots, \mathbf{f}_{L_1}(\varphi_{L'_1})]$  (or  $\mathbf{A}_{R,v}(\boldsymbol{\varsigma}) \triangleq [\mathbf{f}_{L_2}(\varsigma_1), \dots, \mathbf{f}_{L_2}(\varsigma_{L'_2})]$ ) is an over-complete horizontal (or vertical) array response; and  $\mathbf{S} \in \mathbb{C}^{M' \times L'}$  is the corresponding channel coefficient matrix in the angular domain with  $L' = L'_1 L'_2$ . Experimental studies have shown that the propagation channel often exhibits limited scattering geometry [20]. As a consequence, only a few entries of  $\mathbf{S}$  are nonzero with each corresponding

<sup>1</sup>The assumption of the knowledge of  $\bar{\mathbf{H}}_{RB}$  does not lose any generality since any possible error in the channel averaging process can be absorbed into  $\bar{\mathbf{H}}_{RB}$ .

to a channel path. That is,  $\mathbf{S}$  is a sparse matrix. Similarly to (8),  $\mathbf{h}_{UR,k}$  is given by

$$\mathbf{h}_{UR,k} = \mathbf{A}_R(\boldsymbol{\varphi}, \boldsymbol{\varsigma}) \mathbf{g}_k, \quad (9)$$

where  $\mathbf{g}_k \in \mathbb{C}^{L' \times K}$  is a sparse vector representing the channel coefficients in the angular domain. We note that the sparsity of  $\mathbf{S}$  and  $\{\mathbf{g}_k\}$  plays an important role in our channel estimation design.

### C. Cascaded Channel Estimation

To facilitate RIS channel estimation, users simultaneously transmit training sequences with length  $T$  to the BS. Denote by  $\mathbf{x}_k = [x_{k1}, \dots, x_{kT}]^T$  the training sequence of user  $k$ , where  $x_{kt}$  is the training symbol of user  $k$  in time slot  $t$ . We assume that the users transmit at constant power  $\tau_X$ , i.e.,  $\mathbb{E}[|x_{kt}|^2] = \tau_X, \forall k, t$ . Over the time duration  $T$ , all the RIS elements are turned on and are set to have the same phase shift. Without loss of generality, we assume that  $\psi(t) = \mathbf{1}, 1 \leq t \leq T$ . Then, the received signal at the BS in time slot  $t$  is given by

$$\mathbf{y}_0(t) = \sum_{k=1}^K (\mathbf{h}_{UB,k} + \mathbf{H}_{RB} \mathbf{h}_{UR,k}) x_{kt} + \mathbf{n}(t), 1 \leq t \leq T, \quad (10)$$

where  $\mathbf{n}(t)$  is an additive white Gaussian noise (AWGN) vector following the distribution of  $\mathcal{CN}(\mathbf{0}, \tau_N \mathbf{I})$ . We assume that all the direct links  $\{\mathbf{h}_{UB,k}\}$  are accurately estimated before the RIS channel estimation procedure, and thus are canceled in (10).<sup>2</sup> Collecting all the received signals in time duration  $T$  and canceling the direct channel links, we rewrite (10) in a matrix form as

$$\mathbf{Y} = \mathbf{H}_{RB} \mathbf{H}_{UR} \mathbf{X} + \mathbf{N}, \quad (11)$$

where  $\mathbf{X} = [\mathbf{x}_1, \dots, \mathbf{x}_K]^T$ ;  $\mathbf{Y} = [\mathbf{y}_0(1), \dots, \mathbf{y}_0(T)] - [\mathbf{h}_{UB,1}, \dots, \mathbf{h}_{UB,K}] \mathbf{X}$ ;  $\mathbf{H}_{UR} = [\mathbf{h}_{UR,1}, \dots, \mathbf{h}_{UR,K}]$ ; and  $\mathbf{N} = [\mathbf{n}(1), \dots, \mathbf{n}(T)]$ . From (1), (8), and (9), we obtain the system model as

$$\mathbf{Y} = \left( \sqrt{\frac{\kappa}{\kappa+1}} \bar{\mathbf{H}}_{RB} + \mathbf{A}_B \mathbf{S} \mathbf{A}_R^H \right) \mathbf{A}_R \mathbf{G} \mathbf{X} + \mathbf{N} = (\mathbf{H}_0 + \mathbf{A}_B \mathbf{S} \mathbf{R}) \mathbf{G} \mathbf{X} + \mathbf{N}, \quad (12)$$

where we drop the arguments  $\boldsymbol{\vartheta}$ ,  $\boldsymbol{\varphi}$ , and  $\boldsymbol{\varsigma}$  in  $\mathbf{A}_B$  and  $\mathbf{A}_R$  for ease of notation;  $\mathbf{G} \triangleq [\mathbf{g}_1, \dots, \mathbf{g}_K] \in \mathbb{C}^{L' \times K}$ ;  $\mathbf{H}_0 \triangleq \sqrt{\kappa/(\kappa+1)} \bar{\mathbf{H}}_{RB} \mathbf{A}_R \in \mathbb{C}^{M \times L'}$ ; and  $\mathbf{R} \triangleq \mathbf{A}_R^H \mathbf{A}_R \in \mathbb{C}^{L' \times L'}$ .

Upon the reception of  $\mathbf{Y}$  in (12), the BS aims to factorize the channel matrices  $\mathbf{S}$  and  $\mathbf{G}$  with the knowledge of the training signal matrix  $\mathbf{X}$ . Once the angular bases  $\mathbf{A}_B$  and  $\mathbf{A}_R$  are

<sup>2</sup>By turning off the RIS reflecting elements, the estimation of  $\{\mathbf{h}_{UB,k}\}$  can be done by using conventional channel estimation methods for multiuser MIMO systems.



predetermined and the slow-varying component matrix  $\bar{\mathbf{H}}_{RB}$  is given, the sensing matrices  $\mathbf{A}_B$ ,  $\mathbf{H}_0$ , and  $\mathbf{R}$  are also known to the BS. We refer to the above problem as *matrix-calibration* based cascaded channel estimation, since this problem bears some similarity to the blind matrix calibration (BMC) problem [21].

*Remark 1.* The BMC problem in [21] is defined as to calibrate  $\mathbf{A}$  and estimate  $\mathbf{B}$  from a noisy observation of the product  $\mathbf{AB}$ , where the dictionary  $\mathbf{A}$  is partially known. That is,  $\mathbf{A} = \mathbf{A}_0 + \mathbf{A}_1$  with the known part  $\mathbf{A}_0$  and the unknown perturbation  $\mathbf{A}_1$ . Rigorously speaking, the problem in (12) is not exactly a BMC problem. The difference is two-fold: First, in (12), the observation of the matrix product  $\mathbf{Z} = (\mathbf{H}_0 + \mathbf{A}_B \mathbf{S} \mathbf{R}) \mathbf{G}$  is through a linear system  $\mathbf{Y} = \mathbf{Z} \mathbf{X} + \mathbf{N}$ . In BMC,  $\mathbf{X}$  is limited to  $\mathbf{X} = \mathbf{I}$ . Second, BMC often assumes an independent and identically distributed (i.i.d.) Gaussian distribution for perturbation  $\mathbf{A}_1$  [21], [22], whereas we exploit the hidden sparsity of the perturbation matrix under the domain transformed by  $\mathbf{A}_B$  and  $\mathbf{R}$  in (12). As aforementioned, such a sparse representation of the perturbation models the fast channel variation in the RIS-to-BS link.

### III. MATRIX-CALIBRATION BASED CASCADED CHANNEL ESTIMATION ALGORITHM

In this section, we first derive the posterior mean estimators of  $\mathbf{S}$  and  $\mathbf{G}$  given  $\mathbf{Y}$  in (12) under the Bayesian inference framework. We then resort to sum-product message passing to compute the estimators. To reduce the computational complexity, we impose additional approximations to simplify the message updates in the large-system limit. Finally, we discuss useful modifications to enhance the robustness of the proposed algorithm in practical implementation.

#### A. Bayesian Inference

Define  $\mathbf{W} \triangleq \mathbf{H}_0 + \mathbf{A}_B \mathbf{S} \mathbf{R}$ ,  $\mathbf{Z} \triangleq \mathbf{W} \mathbf{G}$ , and  $\mathbf{Q} \triangleq \mathbf{Z} \mathbf{X}$ . Under the assumption of AWGN, we have

$$p(\mathbf{Y}|\mathbf{Q}) = \prod_{m=1}^M \prod_{t=1}^T p(y_{mt}|q_{mt}) = \prod_{m=1}^M \prod_{t=1}^T \mathcal{CN}(y_{mt}; q_{mt}, \tau_N). \quad (13)$$

Motivated by the sparsity of  $\mathbf{S}$  and  $\mathbf{G}$ , we employ Bernoulli-Gaussian distributions to model their prior distributions as

$$p(\mathbf{S}) = \prod_{m'=1}^{M'} \prod_{l'=1}^{L'} p(s_{m'l'}) = \prod_{m'=1}^{M'} \prod_{l'=1}^{L'} (1 - \lambda_S) \delta(s_{m'l'}) + \lambda_S \mathcal{CN}(s_{m'l'}; 0, \tau_S), \quad (14)$$

$$p(\mathbf{G}) = \prod_{l=1}^{L'} \prod_{k=1}^K p(g_{lk}) = \prod_{l=1}^{L'} \prod_{k=1}^K (1 - \lambda_G) \delta(g_{lk}) + \lambda_G \mathcal{CN}(g_{lk}; 0, \tau_G), \quad (15)$$

where  $\lambda_S$  (or  $\lambda_G$ ) is the corresponding Bernoulli parameter of  $\mathbf{S}$  (or  $\mathbf{G}$ ); and  $\tau_S$  (or  $\tau_G$ ) is the variance of the nonzero entries of  $\mathbf{S}$  (or  $\mathbf{G}$ ). From Bayes' theorem, the posterior distribution  $p(\mathbf{S}, \mathbf{G}|\mathbf{Y})$  is given by

$$p(\mathbf{S}, \mathbf{G}|\mathbf{Y}) = \frac{1}{p(\mathbf{Y})} p(\mathbf{Y}|\mathbf{S}, \mathbf{G}) p(\mathbf{S}) p(\mathbf{G}). \quad (16)$$

With (16), the posterior mean estimators of  $\mathbf{S}$  and  $\mathbf{G}$  are given by  $\hat{\mathbf{S}} = [\hat{s}_{m'l'}]$  and  $\hat{\mathbf{G}} = [\hat{g}_{lk}]$ , where

$$\hat{s}_{m'l'} = \int s_{m'l'} p(s_{m'l'}|\mathbf{Y}) ds_{m'l'}, \quad \hat{g}_{lk} = \int g_{lk} p(g_{lk}|\mathbf{Y}) dg_{lk}. \quad (17)$$

In the above,  $p(s_{m'l'}|\mathbf{Y}) = \int \int p(\mathbf{S}, \mathbf{G}|\mathbf{Y}) d\mathbf{G} d(\mathbf{S} \setminus s_{m'l'})$  and  $p(g_{lk}|\mathbf{Y}) = \int \int p(\mathbf{S}, \mathbf{G}|\mathbf{Y}) d\mathbf{S} d(\mathbf{G} \setminus g_{lk})$  are the marginal distributions with respect to  $s_{m'l'}$  and  $g_{lk}$ , respectively, where  $\mathbf{X} \setminus x_{ij}$  means the collection of the elements of matrix  $\mathbf{X}$  except for the  $(i, j)$ -th one. The posterior mean estimators in (17) achieve the minimum mean square errors (MMSEs) [23] defined as

$$\text{MMSE}_{\mathbf{S}} = \frac{1}{M'L'} \mathbb{E} [\|\mathbf{S} - \hat{\mathbf{S}}\|_F^2], \quad \text{MMSE}_{\mathbf{G}} = \frac{1}{L'K} \mathbb{E} [\|\mathbf{G} - \hat{\mathbf{G}}\|_F^2], \quad (18a)$$

where the expectations are taken over the joint distribution of  $\mathbf{S}$ ,  $\mathbf{G}$ , and  $\mathbf{Y}$ . Exact evaluation of  $\hat{\mathbf{S}}$  and  $\hat{\mathbf{G}}$  are generally intractable due to the high-dimensional integrations involved in the marginalization. In the following, we provide an approximate solution by following the message passing principle.

### B. Message Passing for Marginal Posterior Computation

Plugging (13)–(15) into (16), we obtain

$$\begin{aligned} p(\mathbf{S}, \mathbf{G}|\mathbf{Y}) = & \frac{1}{p(\mathbf{Y})} \left( \prod_{m=1}^M \prod_{t=1}^T \mathcal{CN}(y_{mt}; q_{mt}, \tau_N) \delta \left( q_{mt} - \sum_{k=1}^K z_{mk} x_{kt} \right) \right) \\ & \left( \prod_{m=1}^M \prod_{k=1}^K \delta \left( z_{mk} - \sum_{l=1}^{L'} w_{ml} g_{lk} \right) \right) \left( \prod_{m=1}^M \prod_{l=1}^{L'} \delta \left( w_{ml} - h_{0,ml} - \sum_{m'=1}^{M'} \sum_{l'=1}^{L'} a_{B,mm'} s_{m'l'} r_{l'l} \right) \right) \\ & \left( \prod_{l=1}^{L'} \prod_{k=1}^K (1 - \lambda_G) \delta(g_{lk}) + \lambda_G \mathcal{CN}(g_{lk}; 0, \tau_G) \right) \left( \prod_{m'=1}^{M'} \prod_{l'=1}^{L'} (1 - \lambda_S) \delta(s_{m'l'}) + \lambda_S \mathcal{CN}(s_{m'l'}; 0, \tau_S) \right). \end{aligned} \quad (19)$$

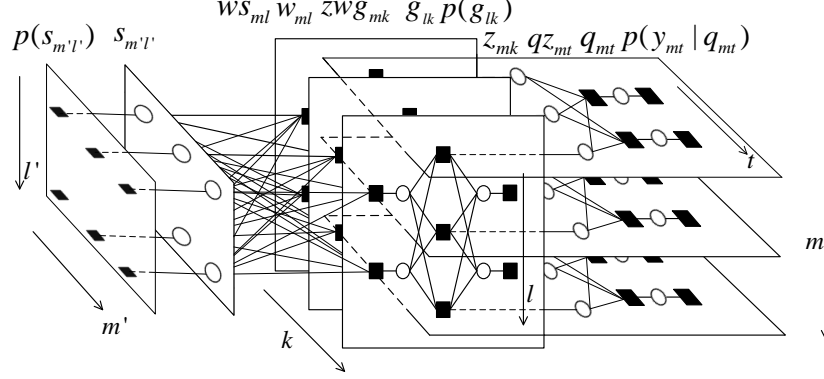


Fig. 2. An illustration of the factor graph representation for  $M = M' = K = 3$  and  $T = L' = 2$ , where blank circles and black squares represent variable nodes and factor nodes, respectively.

We construct a factor graph to represent (19) and apply the canonical message passing algorithm to approximately compute the estimators in (17). The factor graph is depicted in Fig. 2. The variables  $S$ ,  $G$ ,  $W$ ,  $Z$ , and  $Q$  are represented by the variable nodes  $\{s_{m'l'}\}_{1 \leq m' \leq M', 1 \leq l' \leq L'}$ ,  $\{g_{lk}\}_{1 \leq l \leq L', 1 \leq k \leq K}$ ,  $\{w_{ml}\}_{1 \leq m \leq M, 1 \leq l \leq L'}$ ,  $\{z_{mk}\}_{1 \leq m \leq M, 1 \leq k \leq K}$ , and  $\{q_{mt}\}_{1 \leq m \leq M, 1 \leq t \leq T}$ , respectively. The factorizable pdfs in (19), represented by factor nodes  $\{p(s_{m'l'})\}_{1 \leq m' \leq M', 1 \leq l' \leq L'}$ ,  $\{p(g_{lk})\}_{1 \leq l \leq L', 1 \leq k \leq K}$ ,  $\{ws_{ml}\}_{1 \leq m \leq M, 1 \leq l \leq L'}$ ,  $\{zwg_{mk}\}_{1 \leq m \leq M, 1 \leq k \leq K}$ ,  $\{qz_{mt}\}_{1 \leq m \leq M, 1 \leq t \leq T}$ , and  $\{p(y_{mt}|q_{mt})\}_{1 \leq m \leq M, 1 \leq t \leq T}$ , are connected to their associated arguments. We summarize the notation of the factor nodes in Table I. Denote by  $\Delta_{a \rightarrow b}^i(\cdot)$  the message from node  $a$  to  $b$  in iteration  $i$ , and by  $\Delta_c^i(\cdot)$  the marginal message computed at variable node  $c$  in iteration  $i$ . Applying the sum-product rule, we obtain the following messages:

1) *Messages between  $\{qz_{mt}\}$  and  $\{z_{mk}\}$ :* For  $1 \leq m \leq M, 1 \leq t \leq T, 1 \leq k \leq K$ ,

$$\Delta_{qz_{mt} \rightarrow z_{mk}}^i(z_{mk}) \propto \int p\left(y_{mt} \mid \sum_{k=1}^K z_{mk} x_{kt}\right) \prod_{j \neq k} \left(\Delta_{z_{mj} \rightarrow qz_{mt}}^i(z_{mj}) dz_{mj}\right), \quad (20)$$

$$\Delta_{z_{mk} \rightarrow qz_{mt}}^{i+1}(z_{mk}) \propto \mathcal{P}_{z_{mk}}^i(z_{mk}) \prod_{j \neq t} \Delta_{qz_{mj} \rightarrow z_{mk}}^i(z_{mk}), \quad (21)$$

where the auxiliary distribution  $\mathcal{P}_{z_{mk}}^i(z_{mk})$  is defined as

$$\mathcal{P}_{z_{mk}}^i(z_{mk}) \propto \int \delta\left(z_{mk} - \prod_{l=1}^{L'} w_{ml} g_{lk}\right) \prod_{l=1}^{L'} (\Delta_{w_{ml} \rightarrow zwg_{mk}}^i(w_{ml}) \Delta_{g_{lk} \rightarrow zwg_{mk}}^i(g_{lk}) dw_{ml} dg_{lk}). \quad (22)$$

TABLE I  
NOTATION OF FACTOR NODES

Factor	Distribution	Exact Form
$p(s_{m'l'})$	$p(s_{m'l'})$	$(1 - \lambda_S)\delta(s_{m'l'}) + \lambda_S \mathcal{CN}(s_{m'l'}; 0, \tau_S)$
$p(g_{lk})$	$p(g_{lk})$	$(1 - \lambda_G)\delta(g_{lk}) + \lambda_G \mathcal{CN}(g_{lk}; 0, \tau_G)$
$w_{s_{ml}}$	$p(w_{ml} s_{m'l'}, \forall m', \forall l')$	$\delta(w_{ml} - h_{0,ml} - \sum_{m'=1}^{M'} \sum_{l'=1}^{L'} a_{B,mm'} s_{m'l'} r_{l'l})$
$zw_{g_{mk}}$	$p(z_{mk} w_{ml}, g_{lk}, \forall l)$	$\delta(z_{mk} - \sum_{l=1}^{L'} w_{ml} g_{lk})$
$qz_{mt}$	$p(q_{mt} z_{mk}, \forall k)$	$\delta(q_{mt} - \sum_{k=1}^K z_{mk} x_{kt})$
$p(y_{mt} q_{mt})$	$p(y_{mt} q_{mt})$	$\mathcal{CN}(y_{mt}; q_{mt}, \tau_N)$

2) *Messages between  $\{g_{lk}\}$  and  $\{zw_{g_{mk}}\}$ :* For  $1 \leq l \leq L', 1 \leq m \leq M, 1 \leq k \leq K$ ,

$$\Delta_{zw_{g_{mk}} \rightarrow g_{lk}}^i(g_{lk}) \propto \int \prod_{j \neq l} \left( \Delta_{g_{jk} \rightarrow zw_{g_{mk}}}^i(g_{jk}) dg_{jk} \right) \prod_{l=1}^{L'} \left( \Delta_{w_{ml} \rightarrow zw_{g_{mk}}}^i(w_{ml}) dw_{ml} \right) \prod_{t=1}^T \Delta_{qz_{mt} \rightarrow z_{mk}}^i(z_{mk}) \delta \left( z_{mk} - \sum_{l=1}^{L'} w_{ml} g_{lk} \right) dz_{mk}, \quad (23)$$

$$\Delta_{g_{lk} \rightarrow zw_{g_{mk}}}^{i+1}(g_{lk}) \propto p(g_{lk}) \prod_{j \neq m} \Delta_{zw_{g_{jk}} \rightarrow g_{lk}}^i(g_{lk}). \quad (24)$$

3) *Messages between  $\{w_{ml}\}$  and  $\{zw_{g_{mk}}\}$ :* For  $1 \leq l \leq L', 1 \leq m \leq M, 1 \leq k \leq K$ ,

$$\Delta_{zw_{g_{mk}} \rightarrow w_{ml}}^i(w_{ml}) \propto \int \prod_{l=1}^{L'} \left( \Delta_{g_{lk} \rightarrow zw_{g_{mk}}}^i(g_{lk}) dg_{lk} \right) \prod_{j \neq l} \left( \Delta_{w_{mj} \rightarrow zw_{g_{mk}}}^i(w_{mj}) dw_{mj} \right) \prod_{t=1}^T \Delta_{qz_{mt} \rightarrow z_{mk}}^i(z_{mk}) \delta \left( z_{mk} - \sum_{l=1}^{L'} w_{ml} g_{lk} \right) dz_{mk}, \quad (25)$$

$$\Delta_{w_{ml} \rightarrow zw_{g_{mk}}}^{i+1}(w_{ml}) \propto \mathcal{P}_{w_{ml}}^i(w_{ml}) \prod_{j \neq k} \Delta_{zw_{g_{mj}} \rightarrow w_{ml}}^i(w_{ml}), \quad (26)$$

where

$$\mathcal{P}_{w_{ml}}^i(w_{ml}) \propto \int \delta \left( w_{ml} - h_{0,ml} - \sum_{m'=1}^{M'} \sum_{l'=1}^{L'} a_{B,mm'} s_{m'l'} r_{l'l} \right) \prod_{m'=1}^{M'} \prod_{l'=1}^{L'} \left( \Delta_{s_{m'l'} \rightarrow w_{s_{ml}}}^i(s_{m'l'}) ds_{m'l'} \right). \quad (27)$$

TABLE II  
NOTATIONS OF MEANS AND VARIANCES FOR MESSAGES

Message	Mean	Variance
$\Delta_{g_{lk} \rightarrow zw_{g_{mk}}}^i(g_{lk})$	$\hat{g}_{lk,m}(i)$	$v_{lk,m}^g(i)$
$\Delta_{s_{m'l'} \rightarrow ws_{ml}}^i(s_{m'l'})$	$\hat{s}_{m'l',ml}(i)$	$v_{m'l',ml}^s(i)$
$\Delta_{w_{ml} \rightarrow zw_{g_{mk}}}^i(w_{ml})$	$\hat{w}_{ml,k}(i)$	$v_{ml,k}^w(i)$
$\Delta_{z_{mk} \rightarrow qz_{mt}}^i(z_{mk})$	$\hat{z}_{mk,t}(i)$	$v_{mk,t}^z(i)$
$\Delta_{g_{lk}}^i(g_{lk})$	$\hat{g}_{lk}(i)$	$v_{lk}^g(i)$
$\Delta_{s_{m'l'}}^i(s_{m'l'})$	$\hat{s}_{m'l'}(i)$	$v_{m'l'}^s(i)$
$\Delta_{w_{ml}}^i(w_{ml})$	$\hat{w}_{ml}(i)$	$v_{ml}^w(i)$
$\Delta_{z_{mk}}^i(z_{mk})$	$\hat{z}_{mk}(i)$	$v_{mk}^z(i)$

4) *Messages between  $\{s_{m'l'}\}$  and  $\{ws_{ml}\}$ :* For  $1 \leq l, l' \leq L', 1 \leq m' \leq M', 1 \leq m \leq M$ ,

$$\Delta_{ws_{ml} \rightarrow s_{m'l'}}^i(s_{m'l'}) \propto \int dw_{ml} \delta \left( w_{ml} - h_{0,ml} - \sum_{m'=1}^{M'} \sum_{l'=1}^{L'} a_{B,mm'} s_{m'l'} r_{l'l} \right) \prod_{k=1}^K \Delta_{zw_{g_{mk}} \rightarrow w_{ml}}^i(w_{ml}) \prod_{(j,n) \neq (m',l')} \left( \Delta_{s_{jn} \rightarrow ws_{ml}}^i(s_{jn}) ds_{jn} \right), \quad (28)$$

$$\Delta_{s_{m'l'} \rightarrow ws_{ml}}^{i+1}(s_{m'l'}) \propto p(s_{m'l'}) \prod_{(j,n) \neq (m,l)} \Delta_{ws_{jn} \rightarrow s_{m'l'}}^i(s_{m'l'}). \quad (29)$$

5) *Marginal messages at variable nodes:* For  $1 \leq l, l' \leq L', 1 \leq m' \leq M', 1 \leq m \leq M, 1 \leq k \leq K$ ,

$$\Delta_{z_{mk}}^{i+1}(z_{mk}) \propto \mathcal{P}_{z_{mk}}^i(z_{mk}) \prod_{t=1}^T \Delta_{qz_{mt} \rightarrow z_{mk}}^i(z_{mk}), \quad (30)$$

$$\Delta_{w_{ml}}^{i+1}(w_{ml}) \propto \mathcal{P}_{w_{ml}}^i(w_{ml}) \prod_{k=1}^K \Delta_{zw_{g_{mk}} \rightarrow w_{ml}}^i(w_{ml}), \quad (31)$$

$$\Delta_{g_{lk}}^{i+1}(g_{lk}) \propto p(g_{lk}) \prod_{m=1}^M \Delta_{zw_{g_{mk}} \rightarrow g_{lk}}^i(g_{lk}), \quad (32)$$

$$\Delta_{s_{m'l'}}^{i+1}(s_{m'l'}) \propto p(s_{m'l'}) \prod_{m=1}^M \prod_{l'=1}^{L'} \Delta_{ws_{ml} \rightarrow s_{m'l'}}^i(s_{m'l'}). \quad (33)$$

### C. Approximations for Message Passing

The messages and marginals in (20)–(33) are computationally intractable in general due to the high-dimensional integrations and normalizations therein. To tackle this, we simplify the

---

**Algorithm 1:** The Proposed Algorithm
 

---

**Input:**  $\mathbf{Y}; \mathbf{A}_B; \mathbf{H}_0; \mathbf{R}; \mathbf{X}; \tau_N; \lambda_S; \lambda_G; \tau_S; \tau_G$ .

**Initialization:**  $\hat{\gamma}_{mt}(0) = \xi_{mk}(0) = \hat{\alpha}_{mt}(0) = 0$ ;

$\hat{s}_{m'l'}(1)$  randomly drawn from  $p(s_{m'l'})$ ;  $\hat{w}_{ml}(1) = h_{0,ml} + \sum_{m',l'} a_{B,mm'} \hat{s}_{m'l'}(1) r_{l'l}$ ;

$\hat{g}_{lk}(1) = \hat{z}_{mk}(1) = 0$ ;  $v_{m'l'}^s(1) = v_{lk}^g(1) = v_{ml}^w(1) = v_{mk}^z(1) = 1$ .

**for**  $i = 1, 2, \dots, I_{\max}$  **do**

For  $\forall m, k$ , update  $\hat{z}_{mk}$  and  $v_{mk}^z$  by (51), (50), (58), and (49b).

For  $\forall l, k$ , update  $\hat{g}_{lk}$  and  $v_{lk}^g$  by (56), (55a)–(55b), and (57).

For  $\forall m, l$ , update  $\hat{w}_{ml}$  and  $v_{ml}^w$  by (55c)–(55d), (65a), and (66).

For  $\forall m', l'$ , update  $\hat{s}_{m'l'}$  and  $v_{m'l'}^s$  by (65b)–(65c), and (67).

**if**  $\sqrt{\frac{\sum_{m'} \sum_{l'} |\hat{s}_{m'l'}(i+1) - \hat{s}_{m'l'}(i)|^2}{\sum_{m'} \sum_{l'} |\hat{s}_{m'l'}(i)|^2}} \leq \epsilon$  **and**  $\sqrt{\frac{\sum_l \sum_k |\hat{g}_{lk}(i+1) - \hat{g}_{lk}(i)|^2}{\sum_l \sum_k |\hat{g}_{lk}(i)|^2}} \leq \epsilon$  **then**

Stop;

**end if**

**end for**

**Output:**  $\hat{s}_{m'l'}$  and  $\hat{g}_{lk}$ .

---

calculation of (20)–(33) by following the idea of AMP [15], [16] in the large-system limit, i.e.,  $M, M', K, L, L', T \rightarrow \infty$  with the ratios  $M/K$ ,  $M'/K$ ,  $L/K$ ,  $L'/K$ , and  $T/K$  fixed. For ease of notation, we define the means and variances of the messages as in Table II. In the following, we sketch the main approximations involved in the algorithm design, while the detailed derivations can be found in Appendix A.

- A second-order Taylor expansion is adopted to approximate  $\mathcal{P}_{z_{mk}}^i$  as a Gaussian distribution. Moreover, the central limit theorem (CLT) argument [15] approximates  $\prod_{j \neq k} \Delta_{z_{mj} \rightarrow qz_{mt}}^i$  as a Gaussian distribution. Based on these two approximations, we characterize both  $\Delta_{z_{mt} \rightarrow qz_{mk}}^{i+1}$  and  $\Delta_{z_{mk}}^{i+1}$  as Gaussian distributions with tractable means and variances.
- To further reduce the computational complexity, we show that  $\Delta_{z_{mk} \rightarrow qz_{mt}}^{i+1}$  differs from  $\Delta_{z_{mk}}^{i+1}$  in only one term, and this term vanishes in the large-system limit. As a consequence, we use the mean and variance of  $\Delta_{z_{mk}}^{i+1}$  (i.e.,  $\hat{z}_{mk}(i+1)$  and  $v_{mk}^z(i+1)$ ) to approximate those of  $\Delta_{z_{mk} \rightarrow qz_{mt}}^{i+1}$ , and obtain closed-loop updating formulas for  $\hat{z}_{mk}$  and  $v_{mk}^z$ .
- With the tractable form of  $\Delta_{z_{mk}}^{i+1}$ , we show in a similar way that  $\Delta_{w_{ml}}^{i+1}$  can be approximated as a Gaussian distribution. Taking the prior information (14)–(15) into account, we obtain the closed-loop updating formulas for  $\hat{g}_{lk}$ ,  $v_{lk}^g$ ,  $\hat{s}_{m'l'}$  and  $v_{m'l'}^s$ .

We summarize the resultant algorithm in Algorithm 1. Besides, we employ the adaptive damping technique [24] to improve the convergence of Algorithm 1. The details are omitted due to space limitation.

#### IV. MSE ANALYSIS BY REPLICA METHOD

As discussed in Section III-A, the MMSEs in (18) are difficult to evaluate in general. In this section, we derive an asymptotic performance bound of the MSEs under some mild assumptions by employing the replica method from statistical physics [17]. Although some basic assumptions used in the replica method cannot be rigorously justified, this method has proved successful in analyzing bilinear matrix factorization problems [21], [22]. Moreover, the result in [22] is adopted in analyzing the symbol error rate of the massive MIMO systems with low-precision analog-to-digital convertors in [25]. The analysis in this section can be regarded as an extension of the replica framework in [22] to the considered matrix-calibration-based cascaded channel estimation problem in (12).

##### A. Asymptotic MSE Analysis

We assume that the prior distributions (13)–(15) are perfectly known. Furthermore, throughout this subsection, we restrict our analysis to the scenario where both the sampling grids  $\varphi$  and  $\varsigma$  uniformly cover  $[-1, 1]$  with  $L'_1 = L_1$  and  $L'_2 = L_2$ . As a consequence, the array response matrices  $\mathbf{A}_{B,v}$  and  $\mathbf{A}_{B,h}$  in (8) become two normalized discrete Fourier transform (DFT) matrices and we have  $\mathbf{R} = \mathbf{I}$ . Discussions on the case of over-complete sampling bases with  $L'_1 > L_1$  and/or  $L'_2 > L_2$  can be found in the next subsection. Under these assumptions, the analysis is conducted by evaluating the average free entropy in the large-system limit, i.e.,  $M, M', K, L, L', T \rightarrow \infty$  with the ratios  $M/K$ ,  $M'/K$ ,  $L/K$ ,  $L'/K$ , and  $T/K$  fixed. In the sequel, we use  $K \rightarrow \infty$  to denote this limit for convenience. We define the average free entropy as

$$\mathcal{F} \triangleq \lim_{K \rightarrow \infty} \frac{1}{K^2} \mathbb{E}_{\mathbf{Y}} [\ln p(\mathbf{Y})]. \quad (34)$$

As shown in [22], the MMSEs in (18) correspond to a stationary point of  $\mathcal{F}$ . Following the argument in [22], we first transform (34) as

$$\mathcal{F} = \lim_{n \rightarrow 0} \frac{\partial}{\partial n} \lim_{K \rightarrow \infty} \frac{1}{K^2} \ln \mathbb{E}_{\mathbf{Y}} [p^n(\mathbf{Y})]. \quad (35)$$

With (35), we compute  $\ln \mathbb{E}_{\mathbf{Y}} [p^n(\mathbf{Y})] / K^2$  as  $K \rightarrow \infty$  and then compute the derivative with respect to  $n$  with  $n \rightarrow 0$ . Finally, we compute the stationary point of  $\mathcal{F}$  to obtain the values of the MMSEs.

To facilitate the computation, we define the following quantities:

$$Q_S = \lambda_S \tau_S, Q_G = \lambda_G \tau_G, Q_W = \frac{M'}{M} Q_S + \tau_{H_0}, Q_Z = L' Q_W Q_G, \quad (36)$$

where  $\tau_{H_0} \triangleq \mathbb{E}[|h_{0,ml}|^2]$ . Besides, we define two scalar AWGN channels as

$$Y_S = \sqrt{\tilde{m}_S} S + N_S, Y_G = \sqrt{\tilde{m}_G} G + N_G, \quad (37)$$

where  $N_S, N_G \sim \mathcal{CN}(\cdot; 0, 1)$ ;  $S \sim p(S) = (1 - \lambda_S) \delta(S) + \lambda_S \mathcal{CN}(S; 0, \tau_S)$ ; and  $G \sim p(G) = (1 - \lambda_G) \delta(G) + \lambda_G \mathcal{CN}(G; 0, \tau_G)$ . The parameters  $\tilde{m}_S$  and  $\tilde{m}_G$  will be specified later in (39c)–(39d). In other words, we have  $p(Y_S|S) = \mathcal{CN}(Y_S; \sqrt{\tilde{m}_S} S, 1)$  and  $p(Y_G|G) = \mathcal{CN}(Y_G; \sqrt{\tilde{m}_G} G, 1)$ .

From Bayes' theorem, we obtain  $p(S|Y_S) \propto p(S)p(Y_S|S)$  and  $p(G|Y_G) \propto p(G)p(Y_G|G)$ . Similarly to (17), the posterior mean estimators of  $S$  and  $G$  are given by  $\hat{S} = \int S p(S|Y_S) dS$  and  $\hat{G} = \int G p(G|Y_G) dG$ , which has the MSEs given by

$$\text{MSE}_S = \mathbb{E}_{S, Y_S} [ |S - \hat{S}|^2 ], \text{MSE}_G = \mathbb{E}_{G, Y_G} [ |G - \hat{G}|^2 ]. \quad (38)$$

With these definitions, we show in Appendix B that the MMSEs of  $\mathbf{S}$  and  $\mathbf{G}$  in (18) converge to  $\text{MSE}_S$  and  $\text{MSE}_G$  as  $K \rightarrow \infty$ , where  $(\text{MSE}_S, \text{MSE}_G)$  is the solution to the following fixed-point equations:

$$\tilde{m}_Z = \frac{T \tau_X}{\tau_N + K \tau_X (Q_Z - m_Z)}, \quad m_Z = Q_Z - \frac{Q_Z - m_Z}{1 + \tilde{m}_Z (Q_Z - m_Z)}, \quad (39a)$$

$$\tilde{m}_W = \frac{K m_G}{1/\tilde{m}_Z + Q_Z - L' m_W m_G}, \quad m_W = Q_W - \frac{Q_W - m_W}{1 + \tilde{m}_W (Q_W - m_W)}, \quad (39b)$$

$$\tilde{m}_G = \frac{M m_W}{1/\tilde{m}_Z + Q_Z - L' m_W m_G}, \quad m_G = Q_G - \text{MSE}_G, \quad (39c)$$

$$\tilde{m}_S = \frac{1}{1/\tilde{m}_W + Q_W - M' m_S/M}, \quad m_S = Q_S - \text{MSE}_S. \quad (39d)$$

As a result, the estimators in (17) converge to the outputs of the AWGN channels (37) in the large-system limit.

## B. Further Discussions

It is worth noting that the replica method in Appendix B adopts the CLT to approximate  $w_{ml}^{(a)}$ ,  $z_{mk}^{(a)}$ , and  $q_{mt}^{(a)}$  as Gaussian distributions in (75), where  $x^{(a)}$ ,  $0 \leq a \leq n$  is the  $a$ -th replica of random variable  $x$  and follows the same distribution as  $x$ . To apply the CLT, we restrict the



sampling bases  $\mathbf{A}_{B,v}$  and  $\mathbf{A}_{B,h}$  to be two normalized DFT matrices in Section IV-A. In a more general case where  $\mathbf{A}_{B,v}$  and  $\mathbf{A}_{B,h}$  are two over-complete bases, the Gaussian approximations in (75) may be inaccurate and consequently affect the accuracy of the replica method. In this case,  $\text{MSE}_S$  and  $\text{MSE}_G$  in (38) may not exactly correspond to the stationary point of the average free entropy in (34). As a consequence, the performance bound derived in Section IV-A may become loose, as verified by the numerical results presented in the next section.

## V. NUMERICAL RESULTS

### A. Simulation Results Under Channel Generation Model (13)–(15)

We conduct Monte Carlo simulations to verify the analysis in Section IV. In this subsection, we assume that the channel is generated according to the prior distributions in (13)–(15). This allows us to calculate the MMSEs of the cascaded channel estimation problem defined in (18) by using the replica method as in Section IV. Note that  $\text{MSE}_S$  and  $\text{MSE}_G$  in (38) derived by the replica method will be used as a benchmark to evaluate the performance of our proposed algorithm (i.e., Algorithm 1).

We first consider the case with normalized DFT bases  $\mathbf{A}_{B,v}$  and  $\mathbf{A}_{B,h}$ . We set  $M = 1.28K$ ,  $M' = 1.6K$ ,  $T = 1.5K$ ,  $L = L' = 0.5K$ ,  $\lambda_G = 0.1$ ,  $\lambda_S = 0.05$ , and  $\tau_S = \tau_G = \tau_{H_0} = \tau_X = 1$ . Fig. 3 plots the MSE performance versus noise power for  $K = 40$  and  $K = 100$ . We find that the performance of the proposed message passing algorithm closely matches the analytical bound. Notably, the message passing algorithm is only an approximation of the posterior mean estimators whose computation is intractable, not to mention that we have imposed additional approximations to reduce the complexity. We conclude from the observation that the proposed algorithm generally matches the theoretical posterior mean estimators very well in this setting, and that the performance of the posterior mean estimators can be described by the performance bound derived by the replica method.

Then, we simulate on the scenario with two over-complete bases  $\mathbf{A}_{B,v}$  and  $\mathbf{A}_{B,h}$ . Specifically, we set  $L' = 0.7K$  and keep the other parameters unchanged. From Fig. 4, we find that the analytical result has a small gap from the simulation result. As discussed in Section IV-B, this is because the Gaussian approximations in (75) are less accurate, and hence the performance bound derived by the replica method is not as tight as in Fig. 3.

Next, we study the phase transitions of the cascaded channel estimation problem. Here, we say that the estimation of  $\mathbf{S}$  and  $\mathbf{G}$  is successful if  $\text{MSE}_S \leq -20$  dB and  $\text{MSE}_G \leq -20$  dB.

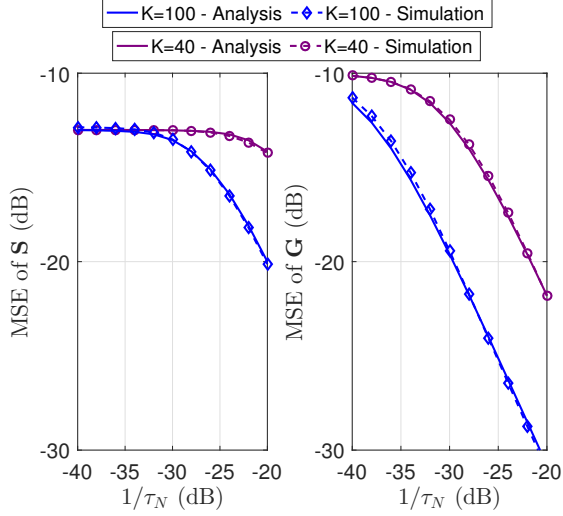


Fig. 3. MSEs versus  $\tau_N$  under normalized DFT bases  $\mathbf{A}_{B,v}$  and  $\mathbf{A}_{B,h}$ . For  $K = 40$ , we set  $L_1 = L'_1 = 4$  and  $L_2 = L'_2 = 5$ ; For  $K = 100$ , we set  $L_1 = L'_1 = 10$  and  $L_2 = L'_2 = 5$ .

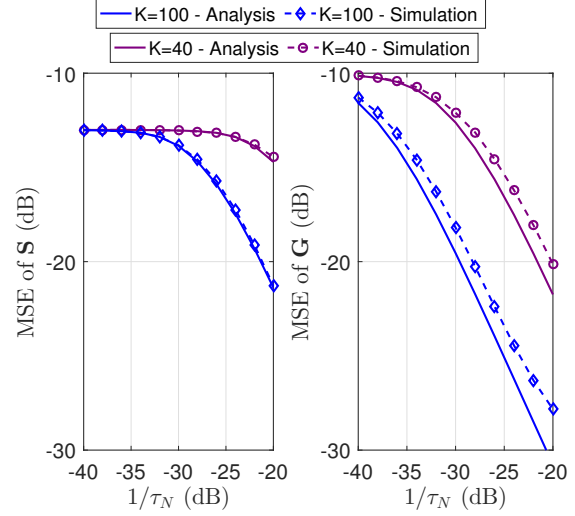


Fig. 4. MSEs versus  $\tau_N$  under over-complete bases  $\mathbf{A}_{B,v}$  and  $\mathbf{A}_{B,h}$ . For  $K = 40$ , we set  $L_1 = L'_1 = 4$ ,  $L_2 = 5$ , and  $L'_2 = 7$ ; For  $K = 100$ , we set  $L_1 = L'_1 = 10$ ,  $L_2 = 5$ , and  $L'_2 = 7$ .

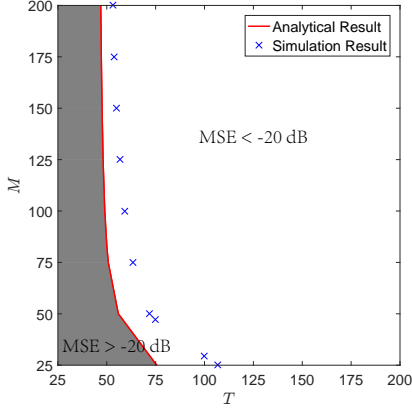


Fig. 5. The phase diagram versus  $M$  and  $T$ . We set  $\tau_N = 15\text{dB}$ ,  $K = 100$ ,  $L = L' = 50$ ,  $M' = 1.25M$ ,  $\lambda_S = 0.05$  and  $\lambda_G = 0.1$ . The red line and the blue cross markers represent the settings that achieve  $-20\text{dB}$  MSEs for the analytical result and Algorithm 1, respectively.

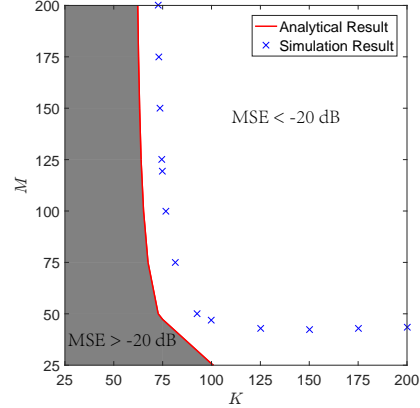


Fig. 6. The phase diagram versus  $M$  and  $K$ . We set  $\tau_N = 15\text{dB}$ ,  $T = 75$ ,  $L = L' = 50$ ,  $M' = 1.25M$ ,  $\lambda_S = 0.05$  and  $\lambda_G = 0.1$ . The red line and the blue cross markers represent the settings that achieve  $-20\text{dB}$  MSEs for the analytical result and Algorithm 1, respectively.

In Fig. 5, we plot the phase transition diagram with varying  $M$  and  $T$  for the analytical MSEs (38) and the empirical MSEs of Algorithm 1 with  $K = 100$  and  $L = 50$ . We find a sharp phase transition for the analytical MSEs at  $T = 50$  and the simulation result requires slightly larger  $M$  and  $T$  to achieve successful estimation. Fig. 5 shows that it is sufficient to have  $M \geq 75$  and  $T \geq 75$  to make the estimation successful in this setting. Note that the state-of-the-art approach [12] estimates the cascaded channels by adopting orthogonal training sequences and turning on

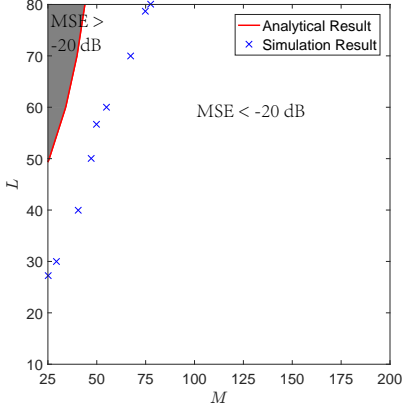


Fig. 7. The phase diagram versus  $M$  and  $L$ . We set  $\tau_N = 15\text{dB}$ ,  $K = 100$ ,  $L' = L$ ,  $M' = 1.25M$ ,  $T = 75$ ,  $\lambda_S = 0.05$  and  $\lambda_G = 0.1$ .

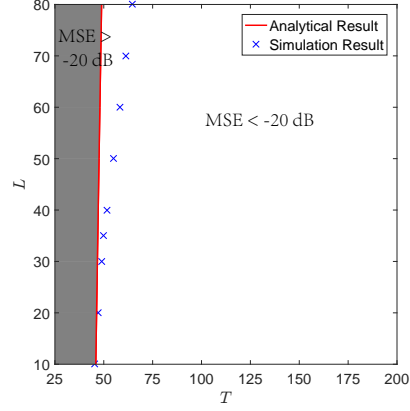


Fig. 8. The phase diagram with various  $T$  and  $L$ . We set  $\tau_N = 15\text{dB}$ ,  $K = 100$ ,  $L' = L$ ,  $M = 150$ ,  $M' = 188$ ,  $\lambda_S = 0.05$  and  $\lambda_G = 0.1$ .

the RIS phase-shift elements sequentially, which generally requires  $T \geq LK = 5000$ . Compared with [12], the proposed algorithm significantly reduces the length of training sequences. Besides, Figs. 6–8 depict the phase transition diagrams with varying  $M$ ,  $L$ ,  $K$ , and  $T$ . We find that the performance of the proposed algorithm is close to the theoretical performance bound in most settings except in the low  $M$  regime. This gap motivates future studies on improved estimation algorithms.

### B. Simulation Results Under a More Realistic Channel Generation Model

We now consider a more realistic channel generation model as follows. We generate  $\tilde{\mathbf{H}}_{RB}$  by (2) with 20 clusters of paths and 10 subpaths per cluster. We draw the central azimuth AoA at the BS of each cluster uniformly over  $[-90^\circ, 90^\circ]$ ; draw the central azimuth (or elevation) AoD at the RIS of each cluster uniformly over  $[-180^\circ, 180^\circ]$  (or  $[-90^\circ, 90^\circ]$ ); and draw each subpath with a  $10^\circ$  angular spread. The channels  $\tilde{\mathbf{H}}_{RB}$  and  $\mathbf{h}_{UR,k}$  are generated by (6)–(7) in a similar way both with a cluster of 10 subpaths. Moreover, every  $\alpha_p$  is drawn from  $\mathcal{CN}(\cdot; 0, 1)$  and is normalized to satisfy  $\|\mathbf{H}_{RB}\|_F^2 = \beta_0 ML$  and  $\|\mathbf{h}_{UR,k}\|_2^2 = \beta_k L$ . We set  $K = 20$ ,  $M = 60$ ,  $T = 35$ ,  $L_1 = L_2 = 4$ ,  $\tau_X = 1$ , and  $\kappa = 9$ . The large-scale fading component is given by  $\beta_i = \beta_{\text{ref}} \cdot d_i^{-\alpha_i}$ , where  $0 \leq i \leq K$ ;  $\beta_{\text{ref}}$  is the reference path loss at the distance 1 meter (m);  $d_i$  is the corresponding link distance; and  $\alpha_i$  is the corresponding pass loss exponent. We set  $\beta_{\text{ref}} = -20$  dB for all the channel links; set  $\alpha_0 = 2$  and  $\alpha_k = 2.6$ ,  $1 \leq k \leq K$ ; and set  $d_0 = 50$  m and  $d_k$  uniformly drawn from  $[10 \text{ m}, 12 \text{ m}]$ .

For the proposed algorithm, we set  $I_{\max} = 2000$  and adopt uniformly sampled over-complete bases in (8)–(9). In specific, we set  $\vartheta$ ,  $\varphi$  and  $\varsigma$  to be uniform sampling grids covering  $[-1, 1]$ . The lengths of the sampling grids are set to have a fixed ratio to the antenna dimensions, i.e.,  $M'/M = L'_1/L_1 = L'_2/L_2 = 2$ , unless otherwise specified. All the results in the sequel are conducted by averaging over 1500 Monte Carlo trials.

Apart from the proposed algorithm, the following baselines are involved for comparisons:

- Concatenate linear regression (LR): By setting aside  $\tilde{\mathbf{H}}_{RB}$ , we first set the estimate of  $\mathbf{H}_{RB}$  as  $\hat{\mathbf{H}}_{RB} = \sqrt{\kappa/(\kappa+1)}\tilde{\mathbf{H}}_{RB}$ , which is deterministic once  $\tilde{\mathbf{H}}_{RB}$  is given. From (12), we obtain the following linear regression problem:

$$\text{vec}(\mathbf{Y}) = (\mathbf{X}^T \otimes \hat{\mathbf{H}}_{RB} \mathbf{A}_R) \text{vec}(\mathbf{G}) + \mathbf{n}', \quad (40)$$

where  $\text{vec}(\cdot)$  represents the vectorization operator, and  $\mathbf{n}'$  represents the effective AWGN. We then infer  $\hat{\mathbf{G}}$  from (40) by employing generalized AMP (GAMP) [16]. Finally, we employ GAMP to estimate  $\tilde{\mathbf{H}}_{RB}$  by solving the resultant LR problem.

- Oracle bound with  $\mathbf{H}_{RB}$  known: Assume that an oracle gives the accurate value of  $\mathbf{H}_{RB}$ . Similarly to (40), we employ GAMP to obtain  $\hat{\mathbf{G}}$  with  $\hat{\mathbf{H}}_{RB} = \mathbf{H}_{RB}$ .
- Sequential channel estimation [12]: The RIS channel estimation are divided into  $L$  phases. At the  $l$ -th phase, we turn off all the RIS elements but the  $l$ -th one. The received signal during the  $l$ -th phase is thus given by  $\mathbf{y}_l = \sum_{k=1}^K \mathbf{h}_{RB,l} h_{UR,k,l} x_{k,l} + \mathbf{n}_l$ , where  $\mathbf{h}_{RB,l}$  is the  $l$ -th column of  $\mathbf{H}_{RB}$  and  $h_{UR,k,l}$  is the  $l$ -th entry of  $\mathbf{h}_{UR,k}$ . With orthogonal training symbols  $\{x_{k,l}\}$ , we can obtain the MMSE estimator of  $\mathbf{h}_{RB,l} h_{UR,k,l}$ .<sup>3,4</sup>

We use the normalized MSEs (NMSEs) of  $\mathbf{H}_{RB}$  and  $\{\mathbf{h}_{UR,k}\}$  to evaluate the performance of the cascaded channel estimation algorithms. Specifically, they are given by

$$\text{NMSE of } \mathbf{H}_{RB} = \frac{\|\hat{\mathbf{H}}_{RB} - \mathbf{H}_{RB}\|_F^2}{\|\mathbf{H}_{RB}\|_F^2}, \quad (41)$$

$$\text{Average NMSE of } \mathbf{h}_{UR,k} = \frac{1}{K} \sum_{k=1}^K \frac{\|\hat{\mathbf{h}}_{UR,k} - \mathbf{h}_{UR,k}\|_2^2}{\|\mathbf{h}_{UR,k}\|_2^2}. \quad (42)$$

<sup>3</sup>This method generally requires  $LK$  time slots for RIS channel estimation. Consider, for example, the system setting described in this subsection, the required length of the training sequence is  $LK = 320 \gg T$ . Here we assume enough training resources for this method *for the comparison purpose*.

<sup>4</sup>This method cannot separate  $\mathbf{h}_{RB,l}$  and  $h_{UR,k,l}$  from the estimate of their product. Here, we assume that  $h_{UR,k,l}$  is given for this method and only exam the estimation error of  $\mathbf{H}_{RB}$  *for the comparison purpose*.

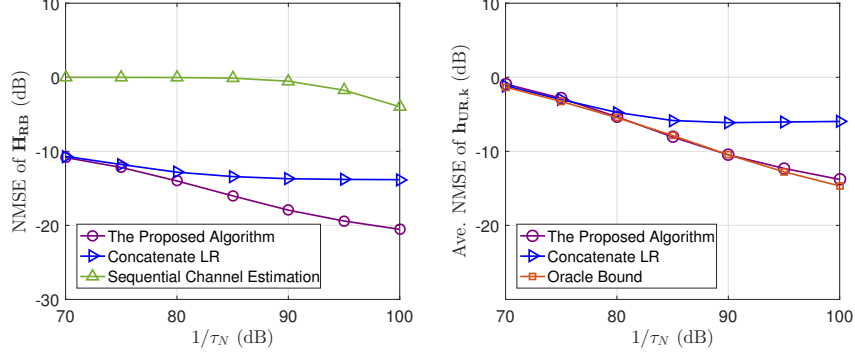


Fig. 9. The NMSE performance versus noise power.

Fig. 9 investigates the RIS channel estimation performance as  $\tau_N$  varies. It can be seen that 1) the proposed algorithm achieves an NMSE of  $\mathbf{h}_{UR,k}$  that is very close to the oracle bound, where the NMSE of  $\mathbf{H}_{RB}$  is assumed to be zero. Moreover, the proposed algorithm outperforms the other baselines in all noise power levels; 2) the sequential channel estimation method has relatively large estimation errors, since it neither exploits the information on the slow-varying channel components nor exploits the hidden channel sparsity; 3) The NMSEs of concatenate LR does not decrease when  $\tau_N \leq -90$  dB. The reason is that the effective noise  $\mathbf{n}'$  in (40) is a combination of the original AWGN noise  $\text{vec}(\mathbf{N})$  and the error resulted from the model mismatch, i.e., the ignored term  $\left(\mathbf{X}^T \otimes \sqrt{1/(\kappa+1)}\tilde{\mathbf{H}}_{RB}\mathbf{A}_R\right)\text{vec}(\mathbf{G})$ . Essentially, the latter term strongly correlates with the variable to be estimated in (40) (i.e.,  $\mathbf{G}$ ). When the model mismatch error dominates the effective noise in the low noise power regime, the correlation issue compromises the convergence of GAMP. On the contrary, the proposed method avoids this problem since the estimate of  $\tilde{\mathbf{H}}_{RB}$ , or equivalently  $\mathbf{S}$ , are updated iteratively during the message passing iteration.

Next, we study the effect of the grid lengths  $M'$ ,  $L'_1$ , and  $L'_2$ . We use  $\eta$  to represent the ratio between the grid length and the number of antennas, i.e.,  $M'/M = L'_1/L_1 = L'_2/L_2 = \eta$ . Fig. 10 plots the NMSEs of the channel estimation algorithms under various  $\eta$ , where  $\tau_N$  is fixed to  $-95$  dB. We have the following observations. 1) The NMSEs of the proposed algorithm, concatenate LR and the oracle estimator decrease as  $\eta$  increases, since increasing the sampling grid length leads to a higher angle resolution and hence a sparser  $\mathbf{S}$  and  $\mathbf{G}$ . 2) The sequential channel estimation method does not exploit the channel sparsity in the angular domain and its performance is invariant to  $\eta$ . 3) The proposed method substantially improves the estimation

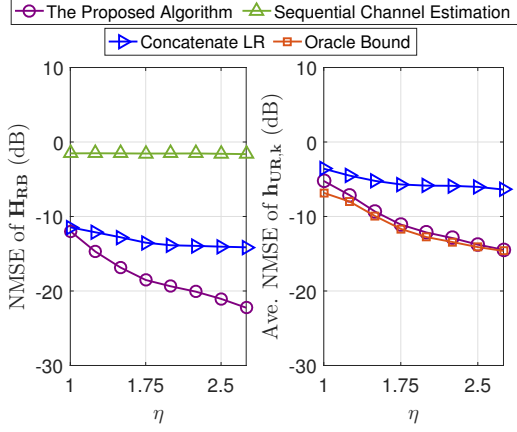


Fig. 10. The NMSE performance versus  $\eta$ , where we set  $\tau_N = -95$  dB.

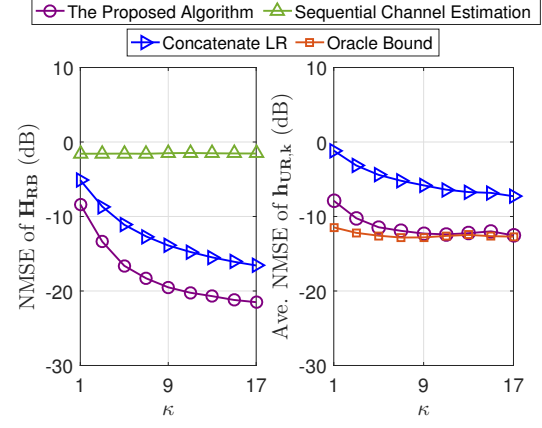


Fig. 11. The NMSE performance versus  $\kappa$  with  $\tau_N = -95$  dB and  $\eta = 2$ .

performance compared to the other algorithms and closely approaches the oracle bound.

In Fig. 11, we study the impact of the Rician factor  $\kappa$  on the channel estimation performance. As  $\kappa$  increases, the portion of the known information in  $\mathbf{H}_{RB}$  increases and hence the NMSEs decrease for all the algorithms except for the sequential channel estimation method, which suffers from the high estimation inaccuracy. Moreover, similarly to Fig. 10, we find the proposed method generally achieves better performance compared to the other channel estimation algorithms.

## VI. CONCLUSIONS

In this paper, we studied the channel estimation problem in the RIS-assisted multiuser MIMO system. We formulated the cascaded channel estimation task as a matrix-calibration based sparse matrix factorization problem by exploiting the knowledge of the slow-varying channel components and the hidden channel sparsity in the angular domain. Then, we proposed a novel message-passing based algorithm to infer the cascaded BS-to-RIS and RIS-to-user channels. Furthermore, we developed a framework to analyze the performance of the considered system. Finally, we used numerical results to confirm the performance improvement of the proposed algorithm compared to the state-of-the-art approach.

## APPENDIX A

1) *Approximation for (20)–(22):* We apply the Fourier inversion theorem to rewrite (22) as

$$\mathcal{P}_{z_{mk}}^i(z_{mk}) \propto \int dt e^{jtz_{mk}} \prod_{l=1}^{L'} (e^{-jtw_{ml}g_{lk}} \Delta_{w_{ml} \rightarrow zw_{g_{mk}}}^i(w_{ml}) \Delta_{g_{lk} \rightarrow zw_{g_{mk}}}^i(g_{lk}) dw_{ml} dg_{lk}). \quad (43)$$

Following the steps in [22, eqs. (51)–(53)], we expand the exponential in the bracket to the second order and simplify (43) as  $\mathcal{P}_{z_{mk}}^i(z_{mk}) \approx \mathcal{CN}(z_{mk}; \hat{p}_{mk}(i), v_{mk}^p(i))$ , where

$$v_{mk}^p(i) = \sum_{l=1}^{L'} (|\hat{w}_{ml,k}(i)|^2 v_{lk,m}^g(i) + v_{ml,k}^w(i) |\hat{g}_{lk,m}(i)|^2 + v_{ml,k}^w(i) v_{lk,m}^g(i)), \quad \hat{p}_{mk}(i) = \sum_{l=1}^{L'} \hat{w}_{ml,k}(i) \hat{g}_{lk,m}(i). \quad (44)$$

Then, we approximate  $q_{mt,k} \triangleq \sum_{j \neq k} z_{mj} x_{jt} \sim \prod_{j \neq k} \Delta_{z_{mj} \rightarrow q_{z_{mt}}}^i$  by the CLT as a Gaussian random variable with mean  $\hat{q}_{mt}(i) - \hat{z}_{mk,t}(i) x_{kt}$  and variance  $v_{mt}^q(i) - v_{mk,t}^z(i) |x_{kt}|^2$ , where  $\hat{q}_{mt}(i) \triangleq \sum_{k=1}^K \hat{z}_{mk,t}(i) x_{kt}$  and  $v_{mt}^q(i) \triangleq \sum_{k=1}^K v_{mk,t}^z(i) |x_{kt}|^2$ . Therefore,

$$\begin{aligned} & \Delta_{q_{z_{mt} \rightarrow z_{mk}}}^i(z_{mk}) \\ & \propto \int dq_{mt,k} \mathcal{CN}(y_{mt}; q_{mt,k} + z_{mk} x_{kt}, \tau_N) \mathcal{CN}(q_{mt,k}; \hat{q}_{mt}(i) - \hat{z}_{mk,t}(i) x_{kt}, v_{mt}^q(i) - v_{mk,t}^z(i) |x_{kt}|^2) \\ & = \mathcal{CN}(y_{mt}; \hat{q}_{mt}(i) + (z_{mk} - \hat{z}_{mk,t}(i)) x_{kt}, \tau_N + v_{mt}^q(i) + (|z_{mk}|^2 - v_{mk,t}^z(i)) |x_{kt}|^2). \end{aligned} \quad (45)$$

Following the steps in [26, eqs. (A.6)–(A.16)], we have

$$\Delta_{q_{z_{mt} \rightarrow z_{mk}}}^{i+1}(z_{mk}) = \mathcal{CN}(z_{mk}; \hat{z}_{mk,t}(i+1), v_{mk,t}^z(i+1)), \quad (46)$$

$$\Delta_{z_{mk}}^{i+1}(z_{mk}) = \mathcal{CN}(z_{mk}; \hat{z}_{mk}(i+1), v_{mk}^z(i+1)), \quad (47)$$

$$\prod_{t=1}^T \Delta_{q_{z_{mt} \rightarrow z_{mk}}}^i(z_{mk}) = \mathcal{CN}(z_{mk}; \hat{e}_{mk}(i), v_{mk}^e(i)), \quad (48)$$

where

$$\hat{z}_{mk,t}(i+1) \approx \hat{z}_{mk}(i+1) - v_{mk}^z(i+1) x_{kt} \hat{\gamma}_{mt}(i), \quad v_{mk,t}^z(i+1) \approx v_{mk}^z(i+1), \quad (49a)$$

$$v_{mk}^z(i+1) = \frac{v_{mk}^p(i) v_{mk}^e(i)}{v_{mk}^p(i) + v_{mk}^e(i)}, \quad \hat{z}_{mk}(i+1) = \frac{v_{mk}^p(i) \hat{e}_{mk}(i) + \hat{p}_{mk}(i) v_{mk}^e(i)}{v_{mk}^p(i) + v_{mk}^e(i)}. \quad (49b)$$

In the above, we introduce the auxiliary variables  $v_{mk}^e(i)$  and  $\hat{e}_{mk}(i)$  as

$$v_{mk}^e(i) = \left( \sum_{t=1}^T v_{mt}^\gamma(i) |x_{kt}|^2 \right)^{-1}, \quad \hat{e}_{mk}(i) = \hat{z}_{mk}(i) + v_{mk}^e(i) \sum_{t=1}^T x_{kt}^* \hat{\gamma}_{mt}(i), \quad (50)$$

where

$$v_{mt}^\beta(i) = \sum_{k=1}^K v_{mk}^z(i) |x_{kt}|^2, \quad \hat{\beta}_{mt}(i) = \sum_{k=1}^K \hat{z}_{mk}(i) x_{kt} - v_{mt}^\beta(i) \hat{\gamma}_{mt}(i-1), \quad (51a)$$

$$v_{mt}^\gamma(i) = \left(v_{mt}^\beta(i) + \tau_N\right)^{-1}, \quad \hat{\gamma}_{mt}(i) = v_{mt}^\gamma(i) \left(y_{mt} - \hat{\beta}_{mt}(i)\right). \quad (51b)$$

2) *Approximation for (23)–(26) and (32):* Plugging (48) into (23) and (25), we have

$$\int dz_{mk} \prod_{t=1}^T \Delta_{qz_{mt} \rightarrow z_{mk}}^i(z_{mk}) \delta\left(z_{mk} - \sum_{l=1}^{L'} w_{ml} g_{lk}\right) = \mathcal{CN}\left(\sum_{l=1}^{L'} w_{ml} g_{lk}; \hat{e}_{mk}(i), v_{mk}^e(i)\right). \quad (52)$$

As a consequence, the forms of (23) and (25) match eq. (13) of [24]. Following the steps in [24, Sec. II-D–Sec. II-E], we obtain

$$\Delta_{g_{lk}}^{i+1}(g_{lk}) = p(g_{lk}) \mathcal{CN}(g_{lk}, \hat{b}_{lk}(i), v_{lk}^b(i)), \quad (53)$$

$$\prod_{k=1}^K \Delta_{zw_{g_{mk}} \rightarrow w_{ml}}^i(w_{ml}) = \mathcal{CN}(w_{ml}, \hat{c}_{ml}(i), v_{ml}^c(i)). \quad (54)$$

In (53)–(54), we introduce

$$v_{lk}^b(i) = \left(\sum_{m=1}^M |\hat{w}_{ml}(i)|^2 v_{mk}^\xi(i)\right)^{-1}, \quad (55a)$$

$$\hat{b}_{lk}(i) = \left(1 - v_{lk}^b(i) \sum_{m=1}^M v_{ml}^w(i) v_{mk}^\xi(i)\right) \hat{g}_{lk}(i) + v_{lk}^b(i) \sum_{m=1}^M \hat{w}_{ml}^*(i) \hat{\xi}_{mk}(i), \quad (55b)$$

$$v_{ml}^c(i) = \left(\sum_{k=1}^K |\hat{g}_{lk}(i)|^2 v_{mk}^\xi(i)\right)^{-1}, \quad (55c)$$

$$\hat{c}_{ml}(i) = \left(1 - v_{ml}^c(i) \sum_{k=1}^K v_{lk}^g(i) v_{mk}^\xi(i)\right) \hat{w}_{ml}(i) + v_{ml}^c(i) \sum_{k=1}^K \hat{g}_{lk}^*(i) \hat{\xi}_{mk}(i), \quad (55d)$$

where

$$v_{mk}^\xi(i) = \frac{v_{mk}^p(i) - v_{mk}^z(i)}{(v_{mk}^p(i))^2}, \quad \hat{\xi}_{mk}(i) = \frac{\hat{z}_{mt}(i) - \hat{p}_{mt}(i)}{v_{mk}^p(i)}. \quad (56a)$$

Plugging (15) into (53), we compute the mean and variance of  $\Delta_{g_{lk}}^{i+1}$  as

$$\hat{g}_{lk}(i+1) = \int g_{lk} \Delta_{g_{lk}}^{i+1}(g_{lk}) dg_{lk}, \quad (57a)$$

$$v_{lk}^g(i+1) = \int g_{lk}^2 \Delta_{g_{lk}}^{i+1}(g_{lk}) dg_{lk} - |\hat{g}_{lk}(i+1)|^2. \quad (57b)$$



Furthermore, following the steps in [24, Sec. II-F], we compute (44) as

$$v_{mk}^p(i) = \sum_{l=1}^{L'} \left( |\hat{w}_{ml}(i)|^2 v_{lk}^g(i) + v_{ml}^w(i) |\hat{g}_{lk}(i)|^2 + v_{ml}^w(i) v_{lk}^g(i) \right), \quad (58a)$$

$$\hat{p}_{mk}(i) = \sum_{l=1}^{L'} \hat{w}_{ml}(i) \hat{g}_{lk}(i) - \hat{\xi}_{mk}(i-1) \sum_{l=1}^{L'} \left( |\hat{w}_{ml}(i)|^2 v_{lk}^g(i) + v_{ml}^w(i) |\hat{g}_{lk}(i)|^2 \right). \quad (58b)$$

3) *Approximation for (27)–(31) and (33):* From (54), we obtain

$$\begin{aligned} \int dw_{ml} \prod_{k=1}^K \Delta_{zwg_{mk} \rightarrow w_{ml}}^i(w_{ml}) \delta \left( w_{ml} - h_{0,ml} - \sum_{m'=1}^{M'} \sum_{l'=1}^{L'} a_{B,mm'} s_{m'l'} r_{l'l} \right) \\ = \mathcal{CN} \left( \hat{c}_{ml}(i); h_{0,ml} + \sum_{m'=1}^{M'} \sum_{l'=1}^{L'} a_{B,mm'} s_{m'l'} r_{l'l}, v_{ml}^c(i) \right). \end{aligned} \quad (59)$$

Plugging (59) into (28), we obtain

$$\Delta_{ws_{ml} \rightarrow s_{m'l'}}^i(s_{m'l'}) \propto \int \mathcal{CN} \left( \hat{c}_{ml}(i); h_{0,ml} + \sum_{m',l'} a_{B,mm'} s_{m'l'} r_{l'l}, v_{ml}^c(i) \right) \prod_{(j,n) \neq (m',l')} \Delta_{s_{jn} \rightarrow ws_{ml}}^i(s_{jn}) ds_{jn}. \quad (60)$$

Define  $\mu_{ml,m'l'} \triangleq \sum_{(j,n) \neq (m',l')} a_{B,mj} s_{jn} r_{nl}$ . By the CLT, we obtain that  $\mu_{ml,m'l'}$  is Gaussian distributed with mean  $\hat{\mu}_{ml}(i) - a_{B,mm'} \hat{s}_{m'l',ml}(i) r_{l'l}$  and variance  $v_{ml}^\mu(i) - a_{B,mm'} v_{m'l',ml}^s(i) r_{l'l}$ , where

$$\hat{\mu}_{ml}(i) = \sum_{m'=1}^{M'} \sum_{l'=1}^{L'} a_{B,mm'} \hat{s}_{m'l',ml}(i) r_{l'l}, \quad v_{ml}^\mu(i) = \sum_{m'=1}^{M'} \sum_{l'=1}^{L'} |a_{B,mm'}|^2 v_{m'l',ml}^s(i) |r_{l'l}|^2. \quad (61a)$$

Therefore, we obtain

$$\begin{aligned} \Delta_{ws_{ml} \rightarrow s_{m'l'}}^i(s_{m'l'}) &\propto \mathbb{E}_{\mu_{ml,m'l'}} [\mathcal{CN}(\hat{c}_{ml}(i); h_{0,ml} + a_{B,mm'} s_{m'l'} r_{l'l} + \mu_{ml,m'l'}, v_{ml}^c(i))] \\ &\propto \mathcal{CN}(\hat{c}_{ml}(i) - h_{0,ml} - a_{B,mm'} s_{m'l'} r_{l'l}; \hat{\mu}_{ml}(i) - a_{B,mm'} \hat{s}_{m'l',ml}(i) r_{l'l}, v_{ml}^\mu(i) + v_{ml}^c(i)) \\ &\propto \exp \left[ -\frac{|a_{B,mm'}|^2 |r_{l'l}|^2}{v_{ml}^\mu(i) + v_{ml}^c(i)} \left| s_{m'l'} - \hat{s}_{m'l'} + \frac{\hat{c}_{ml}(i) - h_{0,ml} - \hat{\mu}_{ml}(i)}{a_{B,mm'} r_{l'l}} \right|^2 \right]. \end{aligned} \quad (62)$$

Following the steps in [26, eqs. (A.6)–(A.16)], we obtain

$$\prod_{m'=1}^{M'} \prod_{l'=1}^{L'} \Delta_{s_{m'l'} \rightarrow ws_{ml}}^i(s_{m'l'}) = \mathcal{CN}(\mu_{ml}; \hat{\mu}_{ml}(i), v_{ml}^\mu(i)), \quad (63)$$

$$\prod_{m=1}^M \prod_{l'=1}^{L'} \Delta_{ws_{ml} \rightarrow s_{m'l'}}^i(s_{m'l'}) = \mathcal{CN}(s_{m'l'}; \hat{d}_{m'l'}(i), v_{m'l'}^d(i)), \quad (64)$$

where

$$v_{ml}^\mu(i) = \sum_{m'=1}^{M'} \sum_{l'=1}^{L'} |a_{B,mm'}|^2 v_{m'l'}^s(i) |r_{l'l}|^2, \quad \hat{\mu}_{ml}(i) = \sum_{m'=1}^{M'} \sum_{l'=1}^{L'} a_{B,mm'} \hat{s}_{m'l'}(i) r_{l'l} - v_{ml}^\mu(i) \hat{\alpha}_{ml}(i-1), \quad (65a)$$

$$v_{ml}^\alpha(i) = (v_{ml}^\mu(i) + v_{ml}^c(i))^{-1}, \quad \hat{\alpha}_{ml}(i) = v_{ml}^\alpha(i) (\hat{c}_{ml}(i) - h_{0,ml} - \hat{\mu}_{ml}(i)), \quad (65b)$$

$$v_{m'l'}^d(i) = \left( \sum_{m=1}^M \sum_{l=1}^{L'} |a_{B,mm'}|^2 v_{ml}^\alpha(i) |r_{l'l}|^2 \right)^{-1}, \quad \hat{d}_{m'l'}(i) = \hat{s}_{m'l'} + v_{m'l'}^d(i) \sum_{m=1}^M \sum_{l=1}^{L'} a_{B,mm'}^* \hat{\alpha}_{ml}(i) r_{l'l}^*. \quad (65c)$$

Plugging (63) into (27) and combining (54), we obtain

$$v_{ml}^w(i+1) = \frac{v_{ml}^\mu(i) v_{ml}^c(i)}{v_{ml}^\mu(i) + v_{ml}^c(i)}, \quad \hat{w}_{ml}(i+1) = \frac{v_{ml}^\mu(i) \hat{c}_{ml}(i) + v_{ml}^c(i) \hat{\mu}_{ml}(i) + v_{ml}^c(i) h_{0,ml}}{v_{ml}^\mu(i) + v_{ml}^c(i)}. \quad (66a)$$

Plugging (64) into (33), we obtain  $\Delta_{s_{m'l'}}^{i+1}(s_{m'l'}) \propto p(s_{m'l'}) \mathcal{CN}(s_{m'l'}; \hat{d}_{m'l'}, v_{m'l'}^d)$  and

$$\hat{s}_{m'l'}(i+1) = \int s_{m'l'} \Delta_{s_{m'l'}}^{i+1}(s_{m'l'}) ds_{m'l'}, \quad (67a)$$

$$v_{m'l'}^s(i+1) = \int s_{m'l'}^2 \Delta_{s_{m'l'}}^{i+1}(s_{m'l'}) ds_{m'l'} - |\hat{s}_{m'l'}(i+1)|^2. \quad (67b)$$

## APPENDIX B

First, note that the replicate partition function  $\mathbb{E}_{\mathbf{Y}}[p^n(\mathbf{Y})]$  is given by

$$\mathbb{E}_{\mathbf{Y}}[p^n(\mathbf{Y})] = \mathbb{E}_{\mathcal{S}, \mathcal{G}, \mathcal{W}, \mathcal{Z}, \mathcal{Q}} \left[ \int d\mathbf{Y} \prod_{a=0}^n p(\mathbf{Y} | \mathbf{Q}^{(a)}) \right], \quad (68)$$

where  $(\cdot)^{(a)}$  is the  $a$ -th replica;  $\mathcal{S} \triangleq \{\mathbf{S}^{(a)} : \forall a\}$ ;  $\mathcal{G} \triangleq \{\mathbf{G}^{(a)} : \forall a\}$ ;  $\mathcal{W} \triangleq \{\mathbf{W}^{(a)} : \forall a\}$ ;  $\mathcal{Z} \triangleq \{\mathbf{Z}^{(a)} : \forall a\}$ ; and  $\mathcal{Q} \triangleq \{\mathbf{Q}^{(a)} : \forall a\}$ . Following [22], we introduce four  $(n+1) \times (n+1)$  auxiliary matrices  $\mathbf{C}_o = [C_o^{ab}]$ ,  $o \in \{S, G, W, Z\}$  that satisfy

$$M' L' \int \prod_{0 \leq a \leq b}^n \delta \left( \sum_{m'l'} \left( s_{m'l'}^{(a)} \right)^* s_{m'l'}^{(b)} - M' L' C_S^{ab} \right) dC_S^{ab} = 1, \quad (69a)$$

$$L' \int \prod_{k=1}^K \prod_{0 \leq a \leq b}^n \delta \left( \sum_l \left( g_{lk}^{(a)} \right)^* g_{lk}^{(b)} - L' C_G^{ab} \right) dC_G^{ab} = 1, \quad (69b)$$

$$M \int \prod_{l=1}^{L'} \prod_{0 \leq a \leq b}^n \delta \left( \sum_m \left( w_{ml}^{(a)} \right)^* w_{ml}^{(b)} - M C_W^{ab} \right) dC_W^{ab} = 1, \quad (69c)$$

$$M \int \prod_{k=1}^K \prod_{0 \leq a \leq b}^n \delta \left( \sum_m \left( z_{mk}^{(a)} \right)^* z_{mk}^{(b)} - M C_Z^{ab} \right) dC_Z^{ab} = 1. \quad (69d)$$

Moreover, we introduce four distributions

$$p(\mathbf{S}|\mathbf{C}_S) = \frac{1}{\mu_S(\mathbf{C}_S)} \prod_{a=0}^n p(\mathbf{S}^{(a)}) \prod_{0 \leq a \leq b}^n \delta \left( \sum_{m'l'} \left( s_{m'l'}^{(a)} \right)^* s_{m'l'}^{(b)} - M' L' C_S^{ab} \right), \quad (70a)$$

$$p(\mathbf{G}|\mathbf{C}_G) = \frac{1}{\mu_G(\mathbf{C}_G)} \prod_{a=0}^n p(\mathbf{G}^{(a)}) \prod_{k=1}^K \prod_{0 \leq a \leq b}^n \delta \left( \sum_l \left( g_{lk}^{(a)} \right)^* g_{lk}^{(b)} - L' C_G^{ab} \right), \quad (70b)$$

$$p(\mathbf{W}|\mathbf{C}_W) = \frac{1}{\mu_W(\mathbf{C}_W)} \prod_{a=0}^n p(\mathbf{W}^{(a)}) \prod_{l=1}^{L'} \prod_{0 \leq a \leq b}^n \delta \left( \sum_m \left( w_{ml}^{(a)} \right)^* w_{ml}^{(b)} - M C_W^{ab} \right), \quad (70c)$$

$$p(\mathbf{Z}|\mathbf{C}_Z) = \frac{1}{\mu_Z(\mathbf{C}_Z)} \prod_{a=0}^n p(\mathbf{Z}^{(a)}) \prod_{k=1}^K \prod_{0 \leq a \leq b}^n \delta \left( \sum_m \left( z_{mk}^{(a)} \right)^* z_{mk}^{(b)} - M C_Z^{ab} \right), \quad (70d)$$

where

$$\mu_S(\mathbf{C}_S) = \mathbb{E}_{\mathbf{S}} \left[ \prod_{0 \leq a \leq b}^n \delta \left( \sum_{m'l'} \left( s_{m'l'}^{(a)} \right)^* s_{m'l'}^{(b)} - M' L' C_S^{ab} \right) \right], \quad (71a)$$

$$\mu_G(\mathbf{C}_G) = \mathbb{E}_{\mathbf{G}} \left[ \prod_{k=1}^K \prod_{0 \leq a \leq b}^n \delta \left( \sum_l \left( g_{lk}^{(a)} \right)^* g_{lk}^{(b)} - L' C_G^{ab} \right) \right], \quad (71b)$$

$$\mu_W(\mathbf{C}_W) = \mathbb{E}_{\mathbf{W}} \left[ \prod_{l=1}^{L'} \prod_{0 \leq a \leq b}^n \delta \left( \sum_m \left( w_{ml}^{(a)} \right)^* w_{ml}^{(b)} - M C_W^{ab} \right) \right], \quad (71c)$$

$$\mu_Z(\mathbf{C}_Z) = \mathbb{E}_{\mathbf{Z}} \left[ \prod_{k=1}^K \prod_{0 \leq a \leq b}^n \delta \left( \sum_m \left( z_{mk}^{(a)} \right)^* z_{mk}^{(b)} - M C_Z^{ab} \right) \right]. \quad (71d)$$

Plugging (69)–(70) into (68), we obtain

$$\begin{aligned} \mathbb{E}_{\mathbf{Y}} [p^n(\mathbf{Y})] &= \int d(M' L' C_S^{ab}) d(L' K C_G^{ab}) d(M L' C_W^{ab}) d(M K C_Z^{ab}) \\ &\quad \mathbb{E}_{\mathbf{Q}|\mathbf{C}_Z} \left[ \int d\mathbf{Y} \prod_{a=0}^n p(\mathbf{Y}|\mathbf{Q}^{(a)}) \right] \mu_S(\mathbf{C}_S) \mu_G(\mathbf{C}_G) \mu_W(\mathbf{C}_W) \mu_Z(\mathbf{C}_Z), \end{aligned} \quad (72)$$

By introducing auxiliary matrices  $\tilde{\mathbf{C}}_o = [\tilde{C}_o^{ab}]$ ,  $o \in \{S, G, W, Z\}$  and applying the saddle point

method, we obtain

$$\ln \mathbb{E}_{\mathbf{Y}} [p^n(\mathbf{Y})] = \text{extr}_{\mathbf{C}_o, \tilde{\mathbf{C}}_o, o \in \{S, G, W, Z\}} \{\mathcal{I}_Q + \mathcal{I}_Z + \mathcal{I}_W + \mathcal{I}_G + \mathcal{I}_S\}, \quad (73)$$

where  $\text{extr}$  is the operation of extremization,

$$\mathcal{I}_Q = MT \cdot \ln \mathbb{E}_{\{q^{(a)}\} | \mathbf{C}_Z} \left[ \int dy \prod_{a=0}^n \mathcal{CN}(y; q^{(a)}, \tau_N) \right], \quad (74a)$$

$$\mathcal{I}_Z = \ln \mathbb{E}_{\mathbf{Z}} \left[ \prod_{k=1}^K e^{\text{tr}(-\tilde{\mathbf{C}}_Z \mathbf{Z}_k^H \mathbf{Z}_k)} \right] + MK \text{tr}(\tilde{\mathbf{C}}_Z \mathbf{C}_Z), \quad (74b)$$

$$\mathcal{I}_W = \ln \mathbb{E}_{\mathbf{W}} \left[ \prod_{l=1}^{L'} e^{\text{tr}(-\tilde{\mathbf{C}}_W \mathbf{W}_l^H \mathbf{W}_l)} \right] + ML' \text{tr}(\tilde{\mathbf{C}}_W \mathbf{C}_W), \quad (74c)$$

$$\mathcal{I}_G = \ln \mathbb{E}_{\mathbf{G}} \left[ \prod_{k=1}^K e^{\text{tr}(-\tilde{\mathbf{C}}_G \mathbf{G}_k^H \mathbf{G}_k)} \right] + L'K \text{tr}(\tilde{\mathbf{C}}_G \mathbf{C}_G), \quad (74d)$$

$$\mathcal{I}_S = \ln \mathbb{E}_{\mathbf{S}} \left[ e^{\text{tr}(-\tilde{\mathbf{C}}_S (\mathbf{S}')^H \mathbf{S}')} \right] + M'L' \text{tr}(\tilde{\mathbf{C}}_S \mathbf{C}_S), \quad (74e)$$

with  $\mathbf{Z}_k = [z_{mk}^{(a)}] \in \mathbb{C}^{(n+1) \times M}$ ,  $\mathbf{W}_l = [w_{ml}^{(a)}] \in \mathbb{C}^{(n+1) \times M}$ ,  $\mathbf{G}_k = [g_{lk}^{(a)}] \in \mathbb{C}^{(n+1) \times L'}$ , and  $\mathbf{S}' = [s_{m'l'}^{(a)}] \in \mathbb{C}^{(n+1) \times M'L'}$ .

To obtain an explicit expression of (73), we further impose the restrictions on  $\mathbf{C}_o, \tilde{\mathbf{C}}_o, o \in \{S, G, W, Z\}$  following the replica symmetry ansatz [22] as  $\mathbf{C}_o = (Q_o + m_o)\mathbf{I} - m_o\mathbf{1}\mathbf{1}^T$  and  $\tilde{\mathbf{C}}_o = (\tilde{Q}_o + \tilde{m}_o)\mathbf{I} - \tilde{m}_o\mathbf{1}\mathbf{1}^T$ . Based on this, we approximate  $w_{ml}^{(a)} = h_{0,ml} + \sum_{m',l'} a_{B,mm'} s_{m'l'}^{(a)} r_{l'l}$ ,  $z_{mk}^{(a)} = \sum_l w_{ml}^{(a)} g_{lk}^{(a)}$ , and  $q_{mt}^{(a)} = \sum_k z_{mk}^{(a)} x_{kt}$  as Gaussian random variables by applying the CLT under the large-system limit. Specifically, we have

$$w_{ml}^{(a)} = \sqrt{Q_w - m_w} u_w^{(a)} + \sqrt{m_w} v_w, \quad (75a)$$

$$z_{mk}^{(a)} = \sqrt{Q_z - m_z} u_z^{(a)} + \sqrt{m_z} v_z, \quad (75b)$$

$$q_{mt}^{(a)} = \sqrt{Q_q - m_q} u_q^{(a)} + \sqrt{m_q} v_q, \quad (75c)$$

where  $u_w^{(a)}, u_z^{(a)}, u_q^{(a)}, v_w, v_z, v_q \sim \mathcal{CN}(\cdot; 0, 1)$ .

Substituting (75) into (74) and noting  $\lim_{n \rightarrow 0} \mathbb{E}_{\mathbf{Y}} [p^n(\mathbf{Y})] = 1$ , we obtain (36) and  $\tilde{Q}_o = 0$ . Finally, by following [25, eqs. (75)–(80)], we compute (35) as

$$\mathcal{F} = \frac{1}{K^2} \text{extr} \left\{ 2MT \cdot \ln \left( \int \mathcal{N}(y; \sqrt{K\tau_X(Q_z - m_z)} u^{(0)} + \sqrt{K\tau_X m_z} v, \tau_N) dy dv du^{(0)} \right) \right\}$$

$$\begin{aligned}
& \cdot \ln \left( \int \mathcal{N} \left( y; \sqrt{K\tau_X(Q_z - m_z)}u + \sqrt{K\tau_X m_z}v, \tau_N \right) Du \right) \\
& + MK \left( \mathbb{E}_{Z^{(0)}} \left[ \int dY_Z e^{-|Y_Z - \sqrt{\tilde{m}_Z} Z^{(0)}|^2} \ln \mathbb{E}_Z \left[ e^{-\tilde{m}_Z |Z|^2 + 2\sqrt{\tilde{m}_Z} \operatorname{Re}(Y_Z^* Z)} \right] \right] - \tilde{m}_Z m_Z \right) \\
& + ML' \left( \mathbb{E}_{W^{(0)}} \left[ \int dY_W e^{-|Y_W - \sqrt{\tilde{m}_W} W^{(0)}|^2} \ln \mathbb{E}_W \left[ e^{-\tilde{m}_W |W|^2 + 2\sqrt{\tilde{m}_W} \operatorname{Re}(Y_W^* W)} \right] \right] - \tilde{m}_W m_W \right) \\
& + L'K \left( \mathbb{E}_{G^{(0)}} \left[ \int dY_G e^{-|Y_G - \sqrt{\tilde{m}_G} G^{(0)}|^2} \ln \mathbb{E}_G \left[ e^{-\tilde{m}_G |G|^2 + 2\sqrt{\tilde{m}_G} \operatorname{Re}(Y_G^* G)} \right] \right] - \tilde{m}_G m_G \right) \\
& + M'L' \left( \mathbb{E}_{S^{(0)}} \left[ \int dY_S e^{-|Y_S - \sqrt{\tilde{m}_S} S^{(0)}|^2} \ln \mathbb{E}_S \left[ e^{-\tilde{m}_S |S|^2 + 2\sqrt{\tilde{m}_S} \operatorname{Re}(Y_S^* S)} \right] \right] - \tilde{m}_S m_S \right) \Bigg\}, \quad (76)
\end{aligned}$$

where  $Dx = dx \cdot e^{-x^2/2}/\sqrt{2\pi}$ , and  $Y_o \in \mathbb{C}, o \in \{S, G, W, Z\}$ . The extremization with respect to  $m_o$  and  $\tilde{m}_o$  yields (39). By evaluating the stationary points of (76), we obtain  $\text{MSE}_S$  and  $\text{MSE}_G$  in (38).

## REFERENCES

- [1] H. Q. Ngo, E. G. Larsson, and T. L. Marzetta, "Energy and spectral efficiency of very large multiuser MIMO systems," *IEEE Trans. Commun.*, vol. 61, no. 4, pp. 1436–1449, Apr. 2013.
- [2] Q. Wu and R. Zhang, "Intelligent reflecting surface enhanced wireless network via joint active and passive beamforming," *IEEE Trans. Wireless Commun.*, vol. 18, no. 11, pp. 5394–5409, Nov. 2019.
- [3] C. Huang, A. Zappone, G. C. Alexandropoulos, M. Debbah, and C. Yuen, "Reconfigurable intelligent surfaces for energy efficiency in wireless communication," *IEEE Trans. Wireless Commun.*, vol. 18, no. 8, pp. 4157–4170, Aug. 2019.
- [4] Q.-U.-A. Nadeem, A. Kammoun, A. Chaaban, M. Debbah, and M.-S. Alouini, "Asymptotic analysis of large intelligent surface assisted MIMO communication," *arXiv preprint arXiv:1903.08127*, 2019.
- [5] C. Liaskos, S. Nie, A. Tsioliaridou, A. Pitsillides, S. Ioannidis, and I. Akyildiz, "A new wireless communication paradigm through software-controlled metasurfaces," *IEEE Commun. Mag.*, vol. 56, no. 9, pp. 162–169, Sep. 2018.
- [6] X. Tan, Z. Sun, D. Koutsonikolas, and J. M. Jornet, "Enabling indoor mobile millimeter-wave networks based on smart reflect-arrays," in *IEEE Conference on Computer Communications (IEEE INFOCOM)*, Apr. 2018, pp. 270–278.
- [7] S. Nie, J. M. Jornet, and I. F. Akyildiz, "Intelligent environments based on ultra-massive MIMO platforms for wireless communication in millimeter wave and terahertz bands," in *Proc. IEEE Int. Conf. Acoust., Speech Signal Process. (ICASSP)*, May 2019, pp. 7849–7853.
- [8] W. Yan, X. Kuai, and X. Yuan, "Passive beamforming and information transfer via large intelligent surface," *arXiv preprint arXiv:1905.01491*, 2019.
- [9] Y. Han, W. Tang, S. Jin, C. Wen, and X. Ma, "Large intelligent surface-assisted wireless communication exploiting statistical csi," *IEEE Trans. Veh. Technol.*, vol. 68, no. 8, pp. 8238–8242, Aug. 2019.
- [10] M. Jung, W. Saad, and G. Kong, "Performance analysis of large intelligent surfaces (LISs): Uplink spectral efficiency and pilot training," *arXiv preprint arXiv:1904.00453*, 2019.
- [11] A. Taha, M. Alrabeiah, and A. Alkhateeb, "Enabling large intelligent surfaces with compressive sensing and deep learning," *arXiv preprint arXiv:1904.10136*, 2019.

- [12] Q.-U.-A. Nadeem, A. Kammoun, A. Chaaban, M. Debbah, and M.-S. Alouini, "Intelligent reflecting surface assisted multi-user MISO communication," *arXiv preprint arXiv:1906.02360*, 2019.
- [13] D. Mishra and H. Johansson, "Channel estimation and low-complexity beamforming design for passive intelligent surface assisted MISO wireless energy transfer," in *Proc. IEEE Int. Conf. Acoust., Speech Signal Process. (ICASSP)*, May 2019, pp. 4659–4663.
- [14] Z.-Q. He and X. Yuan, "Cascaded channel estimation for large intelligent metasurface assisted massive MIMO," *arXiv preprint arXiv:1905.07948*, 2019.
- [15] M. Bayati and A. Montanari, "The dynamics of message passing on dense graphs, with applications to compressed sensing," *IEEE Trans. Inf. Theory*, vol. 57, no. 2, pp. 764–785, Feb. 2011.
- [16] S. Rangan, "Generalized approximate message passing for estimation with random linear mixing," in *Proc. IEEE Int. Symp. Inf. Theory (ISIT)*, Aug. 2011, pp. 2168–2172.
- [17] H. Nishimori, *Statistical Physics of Spin Glasses and Information Processing: An Introduction*. Oxford, U.K.: Oxford Univ. Press, 2001, no. 111 in International Series of Monographs on Physics.
- [18] D. Tse and P. Viswanath, *Fundamentals of Wireless Communication*. New York, NY, USA: Cambridge University Press, 2005.
- [19] X. Li, J. Fang, H. Li, and P. Wang, "Millimeter wave channel estimation via exploiting joint sparse and low-rank structures," *IEEE Trans. Wireless Commun.*, vol. 17, no. 2, pp. 1123–1133, Feb. 2018.
- [20] A. F. Molisch, A. Kuchar, J. Laurila, K. Hugl, and R. Schmalenberger, "Geometry-based directional model for mobile radio channels—principles and implementation," *European Trans. Telecommun.*, vol. 14, no. 4, pp. 351–359, 2003.
- [21] F. Krzakala, M. M'azard, and L. Zdeborov'aa, "Phase diagram and approximate message passing for blind calibration and dictionary learning," in *Proc. IEEE Int. Symp. Inf. Theory (ISIT)*, Jul. 2013, pp. 659–663.
- [22] Y. Kabashima, F. Krzakala, M. Mézard, A. Sakata, and L. Zdeborová, "Phase transitions and sample complexity in Bayes-optimal matrix factorization," *IEEE Trans. Inf. Theory*, vol. 62, no. 7, pp. 4228–4265, Jul. 2016.
- [23] H. V. Poor, *An Introduction to Signal Detection and Estimation*. New York: Springer-Verlag, 1994.
- [24] J. T. Parker, P. Schniter, and V. Cevher, "Bilinear generalized approximate message passing—Part I: Derivation," *IEEE Trans. Signal Process.*, vol. 62, no. 22, pp. 5839–5853, Nov. 2014.
- [25] C. Wen, C. Wang, S. Jin, K. Wong, and P. Ting, "Bayes-optimal joint channel-and-data estimation for massive MIMO with low-precision ADCs," *IEEE Trans. Signal Process.*, vol. 64, no. 10, pp. 2541–2556, May 2016.
- [26] J. Ma, J. Xu, and A. Maleki, "Optimization-based AMP for phase retrieval: The impact of initialization and  $\ell_2$ -regularization," *arXiv preprint arXiv:1801.01170*, 2018.